Structure-factor measurements in ^{4}He at saturated vapor pressure for $1.38 \leq T \leq 4.24$ K

H. N. Robkoff* and R. B. Hallock
Laboratory for Low Temperature Physics, Department of Physics and Astronomy, University of Massachusetts, Amherst, Massachusetts 01003
(Received 16 January 1981)

We present the results of measurements of the liquid structure factor, $S(k)$, for liquid ^{4}He at saturated vapor pressure at seven temperatures between 1.38 and 4.24 K over the momentum-transfer range $k \leq 5.1$ Å^{-1}. The results are compared with previous measurements carried out by both x-ray and neutron scattering techniques. Comparison with recent theoretical work emphasizes the importance of higher-order correlations and more realistic potentials in the description of the liquid. Measurements in the vicinity of the λ transition document a loss in spatial order as the liquid is cooled through T_λ.

I. INTRODUCTION

The microscopic spatial structure of fluids has been a subject of continuing interest for many years and scattering experiments have provided us with a wealth of information in this regard. The presence of a superfluid transition in the case of liquid helium provides us with a unique system for study. Although a temperature-dependent theory of ^{4}He has presented theorists a formidable task, substantial progress has been made during the past 15 years in the development of techniques to study the ground state. Such theoretical work is able to predict the ground-state energy of liquid helium but a much more powerful test is available through the spatial structure.

Correlations among the atoms in the fluid exist since the atoms are of finite size and interact with one another. A measure of the spatial correlations is given by a hierarchy of correlation functions the most important of which is the pair correlation function $g(\vec{r})$. In the case of helium the fluid is isotropic and the pair correlation function is a function of the separation between the atoms alone, thus, we have $g(\vec{r}) \equiv g(r)$. The presence of spatial coherence in the fluid gives rise to structure in the diffraction pattern in a scattering experiment.[1] This structure in the diffraction pattern observed when scattering from a fluid is most often expressed in terms of the liquid structure factor $S(k)$. Here k is the momentum transfer involved in the scattering event. The liquid structure factor is related to the pair correlation function through a Fourier transform,[2]

$$S(k) = 1 + \rho \int e^{i\vec{k}\cdot\vec{r}} [g(r) - 1] d^3r \quad . \tag{1}$$

Here ρ is the density of the fluid under study. It is the function $S(k)$ which provides the direct connection between theory and experiment. All detailed theories which attempt to understand liquid helium in a fundamental way must be able to predict the spatial coherence in the fluid either through $g(r)$ directly or through $S(k)$. Thus, measurements of $S(k)$ provide a crucial testing ground for all such theories.

In the case of x-ray scattering the energy transfer in the scattering from liquid helium is a tiny fraction of the energy of the incident x ray. For this reason the energy change encountered in the scattering event is unresolved by the measurement techniques and the scattering is usually termed elastic although in fact it is not quite so. Quasielastic is a more accurate description. For such a situation, the momentum transfer is related in a simple way to the angle of scatter θ and the wavelength λ of the incident x ray: $k = (4\pi/\lambda)\sin(\theta/2)$. The liquid structure factor is related to the actual scattering intensity by means of an equation which has been written as[3]

$$I(k) = ANT[\sigma_e S(k) + \sigma_i] \quad , \tag{2}$$

where A is the Thomson cross section for photon-electron scattering, N is the number of atoms in the sample which can potentially participate in a scattering event, and T is a transmission factor: atoms deeper within the target see an incident beam of diminished intensity. The scattering by the electrons within a given atom may take place in a coherent way. To account for this the coherent scattering factor σ_e is defined. Other incoherent events (Compton for example) are possible and these are described by the incoherent scattering factor σ_i. The liquid structure factor describes the additional structure in the scattered intensity due to the interatomic spatial correlations in the fluid under study.

We report here measurements of the scattering intensity observed over the momentum transfer interval $0.21 \leq k \leq 5.13$ Å^{-1} at seven temperatures over the range $1.38 \leq T \leq 4.24$ K in the case of liquid ^{4}He. All of the measurements have been done at saturated vapor pressure and the results analyzed to

obtain the liquid structure factor at each temperature studied. In Sec. II the apparatus is described briefly and Sec. III contains a discussion of the data analysis. A discussion of the results and a detailed comparison with other experimental work and recent theoretical predictions is given in Sec. IV. Conclusions are presented in Sec. V.

II. APPARATUS AND PROCEDURE

The measurements reported here were performed on an automated cryogenic x-ray diffractometer which was constructed for this work.[4] As illustrated in Fig. 1, the instrument consists of an x-ray source,[5] incident and exit collimators, cryostat and target cell, and main detector[6] and beam monitors.[7] Because helium scatters x rays weakly, an intense source is needed to obtain accurate results in a reasonable period of time. The source chosen is a rotating anode generator typically operated with an electron current of 160 mA at 50 kV accelerating potential. The anode material is copper and the prominent $K\alpha$ line at 1.54 Å was used in these measurements. A vertical line focus is used in the x-ray tube. The resulting beam is collimated vertically and horizontally to a resolution of $\frac{1}{3}°$ in both arms of the diffractometer. Vertical lead plated knife edge slits and stacked tantalum foil Soller slits are used for collimation. Both collimation tubes are evacuated to eliminate air scatter and attenuation and the position of each slit is reproducibly adjustable in vacuum. The beam enters and leaves the cryostat through high-purity N-50-C beryllium windows[8] selected for low iron content. The exit windows are curved and provide an unobstructed 150° arc. The helium sample is contained in a target cell machined from a solid piece of beryllium. In the region of the beam the cell is 9.5 mm in diameter with a wall thickness of 0.25 mm. Thermal shielding is provided by nesting dewar tails. The 4- and 77-K tails are of heavy copper construction and securely grounded thermally to their respective cryogenic reservoirs. The cryostat itself is a slightly modified[9] commercial (Janis, 20.3-cm-diameter straight bucket) design with a 6-day helium hold time. Temperatures were measured with a calibrated germanium resistance thermometer[10] and monitored with an Allyn-Bradley carbon resistor. The exit collimation tube and main detector, positioned by a goniometer and stepping motor, are step scanned through the scattered beam with an angular accuracy of 0.01°. A dwell time of 600 s at each angle was typical. Beam monitors were located in the incident and scattered beams to record any changes in x-ray beam itensity. These monitors are Xe-CO_2 proportional counters.[7] The main detector is an intrinsic germanium device with a measured energy resolution of 284 eV FWHM (full width at half maximum) at 1.54 Å, which is quite sufficient to separate the $K\alpha$ and $K\beta$ lines. No other monochromitization was used. Pulse height spectra were obtained with a 1024 channel multichannel analyzer and stored on magnetic tape for computer analysis. A digital controller automatically sequenced the apparatus through cycles of data acquisition, data read out, and incrementation of the scattering angle. Further details of the apparatus are available elsewhere.[4]

To extract the structure factor from the observed scattering intensity by means of Eq. (2) is a formidable task. This is the case since Eq. (2) contains the number of scattering centers N and in principle one must be able to count at each angle of scatter the

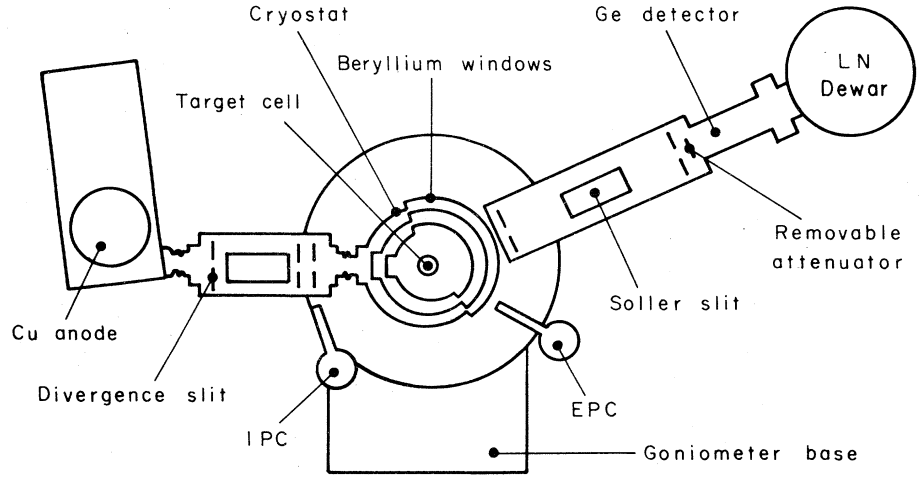

FIG. 1. Schematic top view of the x-ray diffractometer. The notations IPC and EPC refer to incident and exit beam proportional counters which serve to monitor the x-ray beam intensity.

number of helium atoms visible to both the source and detector of scattered x rays. To alleviate this problem Tweet[11] introduced the technique of normalization relative to an ideal gas. One performs the scattering measurement on the system of interest, here ^{4}He, and separately on a sample which is sufficiently close to an ideal gas that one may take $S(k)=1$. Then for the normalization gas

$$I'(k)=AN'T'[\sigma_e'S'(k)+\sigma_i']; \quad S'(k)=1 \tag{3}$$

so that one has

$$S(k)=\frac{I(k)\rho'T'(\sigma_e'+\sigma_i')}{I'(k)\rho T\sigma_e}-\frac{\sigma_i}{\sigma_e}, \tag{4}$$

where the ratio of the number of atoms which participate in the scattering has been replaced by the ratio of the number densities, an accurately measurable quantity. Following Hallock[12] and also Achter and Meyer,[13] neon at 77 K and 1 atm was chosen for this normalization procedure for the work we report here.

The data required are of three kinds: helium scatter, neon normalization, and empty cell scattering. With the target cell at 77 K, empty cell scans were obtained followed by neon data. Additional empty cell scans were taken after removing the neon to verify that no change in cell scatter had occurred. The cell was then cooled to 4 K where further empty cell scans were performed. After all the helium data were obtained, the empty cell was again scanned and warmed to 77 K and additional empty cell and neon data obtained. During a scan the data collected included (at each angle) a pulse height spectrum of the main detector and exit monitor. The incident monitor was also periodically recorded. A typical scan required 12 h.

III. DATA ANALYSIS

The solution of Eq. (4) for the liquid structure factor requires a number of quantities, some of which are determined experimentally, some computed and some available from theory. The primary experimental quantities are the intensities $I(k)$ and $I'(k)$ observed when the x rays are scattered from helium and neon, respectively. As we have mentioned, the use of neon as a second scattering substance obviates the necessity of determining the number of scattering centers and is crucial to the determination of $S(k)$. Without this technique it would be necessary to determine with extreme precision the scattering geometry for each scattering angle. Given the small aberrations present in the geometrical optics such a task would be essentially impossible to carry out to the necessary accuracy. Neon is chosen as the secondary substance since it is very nearly an ideal gas at the easily attainable temperature of liquid nitrogen (77.3 K).

The primary beam provided by the Rigaku RU200PL rotating anode source used for this work consisted of Cu $K\alpha$ and $K\beta$ radiation. The $K\beta$ component, was removed at the detection stage rather than by a crystal monochromator. The intrinsic germanium detector easily resolved the $K\alpha$ and $K\beta$ lines of the copper source as well as some iron fluorescence seen from impurities in the target cell. Monochromatization was accomplished simply by summing only the Cu $K\alpha$ counts which were part of the complete energy spectrum stored on magnetic tape at each scattering angle. Since the resolution of the detector remained stable over the course of the measurements, this was accomplished by simply summing the counts stored over a fixed energy interval.

The output of the x-ray source must remain stable over the long term if one is to avoid spurious effects in the determination of the structure factor. Since this was not the case for our source, it was necessary to monitor the beam intensity continuously. This was accomplished by the use of two Xe-CO_2 proportional counters. One (IPC) was positioned so as to provide a monitor of the incident beam intensity. The other (EPC) monitored the scattered radiation from whichever target sample was in place. The EPC was effective in allowing one to maintain a normalization to constant intensity during the course of a given 12 h scan over all angles. The IPC to be used for interscan normalizations proved on occasion to be unreliable. This was possibly related to temperature changes in the vicinity of the IPC collimation system. Hence, a different but potentially less precise technique was developed to provide normalization to overall constant x-ray intensity. During the course of the measurements scattering from ^{4}He at 2 atm and 4.24 K was periodically done. Thus, throughout the complete data set, the same thermodynamic helium state was repeatedly studied. This fiducial set of scans was adjusted so as to be internally identical and the adjustment factors were applied to the appropriate data sets at other temperatures and densities. By this means overall normalization to constant incident intensity was accomplished.

Since the intensity represented by $I(k)$ and $I'(k)$ is the intensity observed from the helium and neon alone, an empty cell subtraction was also required. To be accurate, the 77- and 4-K empty cell determinations were always done near a fiducial scan and normalized along with the other data. Data scans of the various types were often measured several times in an effort to improve statistics as well as to verify the reproducibility of the data. The empty cell subtraction was done under the assumption that the presence of the target fluid would modify the cell scattering since part of the beam intensity is in fact lost due to the presence of the target sample. Thus, the empty cell correction factor for the wall of the scattering chamber nearest to the detector is slightly less than a

simpler approach would suggest.

Effects due to multiple scattering must also be considered. These are small since the sample transmission is typically 92% but a correction for this effect was made. We follow the procedure of Blech and Averbach[14] who considered the multiple scattering from a cylindrical sample fully bathed in radiation. In the situation appropriate to our work the multiple scattering contribution amounts to a density dependent value in the vicinity of 1% in the case of helium. In the case of neon the multiple scattering correction is negligible. This is due to the fact that in neon a second interaction is much more likely to result in absorption than scattering. In spite of the fact that helium has a nontrivial structure factor which should be taken into account in a proper treatment of multiple scattering effects, the small size of this correction caused us to approximate the multiple scattering correction by this angle independent technique. Evidence from neutron multiple scattering work[15] supports this choice and suggests such coherent effects would be only a small correction to the correction obtained.

The atomic scattering factors σ_e and σ_i Eq. (4) must be obtained from theory. Only a few such theoretical calculations have been carried out for the energies relevant to the work we report here and the results are not in complete agreement. Hence the selection of the scattering factors which we have made requires some discussion. Kim and Inokuti[16] have calculated σ_e and σ_i for the helium atom using a Hartree-Fock wave function and 2, 3, 6, and 20 term Hylleraas wave functions. Rustigi *et al.*[17] computed σ_e with a six term Hylleraas wave function in excellent agreement with the analogous work of Kim and Inokuti.[16] Tavard *et al.*[18] using Hartree-Fock wave functions as given by Clementi reported values of σ_e and σ_i for $Z=1$ and $Z=36$, following the Waller-Hartree method. Hubbell *et al.*[19] have recently computed σ_e and σ_i for $Z=1$ and $Z=100$ in what they regard as a state of the art effort. Now as several authors[16,19] have discussed, Hartree-Fock wave functions produce better one-electron operator expectation values than two-electron values. We note that σ_e depends only on one-electron operators; σ_i is given by two-electron operators. As Kim and Inokuti[16] point out, a more correlated wave function such as the Hylleraas type can be expected to give better values for σ_i. A comparison of the results of these authors and Tavard *et al.*[18] for $k \approx 5$ Å^{-1} reveals a 5% difference in the He inelastic scattering factor. Kim and Inokuti's[16] results agree with the work of Hubbell *et al.* for He and the latter authors and Tavard *et al.*[18] are in good agreement for the case of neon. Kim and Inokuti[16] compare their differential scattering factor results with the measurements by Wollan[20] of the total elastic and inelastic scattering from helium. They find a relativistic correction to σ_i necessary for a good fit to the data at values of k corresponding to the larger momentum transfers explored in the present work. Surprisingly, their Hartree-Fock values compare more favorably with experiment than do their Hylleraas results over the small interval of momentum transfer relevant to this work. They do not offer a resolution of this discrepancy. In view of the above considerations we adopted the neon results of Tavard *et al.*[18] and the values given by Kim and Inokuti[16] for helium.

The inelastic scattering factor just discussed requires a relativistic correction.[1] We have adopted the expression $R=[1+(2h/mc\lambda)\sin^2\theta/2]^{-2}$ rather than the expression of Klein and Nishina[1] with an exponent of -3. The reasons for this choice have been discussed at length by Smelser[21] and will not be repeated here.

The densities of the liquid-helium samples were determined from the known pressure and temperature values at which the measurements were made. For the superfluid state the values of Maynard[22] were used. Maynard[22] reports a precision of 0.3% for his tabulation. Helium densities above the λ transition were obtained from the extensive tabulation due to McCarty.[23] McCarty[23] considers the average error in his tabulation to be 0.5% with a maximum error of at most 1.5%. The work of McCarty[23] is in reasonable agreement with that of both Maynard[22] and Elwell and Meyer[24] in the region of overlap. In the case of neon the density was determined by use of the virial equation and the second virial coefficient of Dymond and Smith.[25] Since neon is very nearly an ideal gas at 77 K and 1 atm, it is not necessary to carry the virial equation beyond the second coefficient.

The observed scattered intensity must be corrected for absorption of the beam within the sample. A narrow beam of x rays passing through a thickness, x, of matter is attenuated according to the well-known[1] expression

$$I(x)=I(0)\exp\left[-\frac{\mu}{\rho}\rho x\right] . \tag{5}$$

The mass absorption coefficient μ/ρ is a strong function of the x-ray energy and the atomic composition of the medium but essentially independent of its physical state. Any mechanism which removes a photon from the incident direction will contribute to the attenuation of the beam and a variety of interactions are possible. At the energy relevant to the present work, the only available processes are scattering and (true) absorption. A scattering event, either Thomson or Compton, will leave a photon in the final state with altered wave vector, whereas absorption, which can occur through the photoelectric effect, leaves an electron but no photon in the final state. A realistic treatment of the attenuation quickly becomes a complex undertaking: one must consider

the effect of the cell, elastic and inelastic scattering must be distinguished carefully (since the diminished photon energy from inelastic events requires use of a somewhat different absorption coefficient), and all paths through the sample and cell are not equally long. Attempts have been made at a thorough analysis[21,26–28] and as it turns out, the complete treatment differs from the naive application of Eq. (21) by only a few percent. As the transmission through either helium or neon amounted to about 92% of the incident beam, the small correction to the straightforward correction is negligible.

The correction adopted for self-absorption therefore was a direct application of Eq. (5) taking the cell diameter as the sample thickness and ignoring effects of the cell itself which are small. Mass absorption coefficients, obtained from the standard reference work,[29] are (for Cu $K\alpha$ radiation): 0.383 for helium and 22.9 for neon in units of cm^2/g. There may be considerable uncertainty in these coefficients,[30] particularly for helium; however, as the amount of absorption is small the results should not be appreciably affected. A careful literature search revealed that no total attenuation measurements of satisfactory precision have ever been performed on helium at these energies[31] so that absorption coefficients must be obtained from semiempirical theoretical calculations.

The considerations discussed above along with Eq. (4) result in a direct determination of the liquid structure factor $S(k)$. In spite of our efforts to ensure overall normalization to constant source intensity, the results were not perfect. At the largest values of the momentum transfer $S(k)$ is required to be unity. Our values as determined from Eq. (4) in some cases differed from unity on the average by several percent. It was decided to impose this condition on the data. Since previous experimental work[32] indicated that beyond $k \simeq 5$ Å^{-1} $S(k)$ was indeed essentially unity, the helium intensity was scaled by an appropriate factor to force the structure factor to unity at large k. Because statistical precision is at its worse in the large-k region, the procedure adopted was to force the arithmetic average of the last five data points to unity. This correction typically required less than a 5% shift in helium intensity. Since $S(k)$ is not exactly unity at $k = 5$ Å^{-1} this procedure will, of course, bias any small scale structure which might, in fact, be present. The effect on the peak height of $S(k)$ from this procedure will be to introduce a systematic shift of not more than $\pm 0.5\%$.

One encounters random, systematic and statistical errors in performing a counting experiment such as this. The most significant of these will now be discussed.

In using neon gas for normalization, it was explicitly assumed that its structure factor was identically unity, as is the case for an ideal gas. The extent of the departure of neon at 1 atm pressure and 77 K from ideality can be discerned by calculating its theoretical structure factor intercept, $S(0) = \rho k_B \chi_T T$. Using the virial equation of state with the second virial coefficient as given by Dymond and Smith,[25] this intercept at 1 atm and 77 K is $S(0) = 1.004$. Therefore, neon departs from ideality by only 0.4% at most and then only at the smallest angles; its structure factor should quickly approach unity with increasing angles of scatter. Hence the use of neon for normalization is well justified and contributes an error of no more than 0.4% at small angles and less elsewhere.

Densities were measured to within 0.5% as were temperatures. The beam width was $\frac{1}{3}°$ or 0.024 Å^{-1} in momentum transfer, although the position of the beam center was reproducible to at least 0.002 Å^{-1}. The theoretical scattering factors are reliable to perhaps 1%. The helium mass absorption coefficient may be in error by as much as 50%, however, that is reflected in the transmission correction by no more than 1.5%. The transmission correction itself was perhaps oversimplified and a more complete treatment may result in changes to $S(k)$ of perhaps 1%, particularly at small angles; the same may be said of the multiple scattering correction.

Drifts in the x-ray source intensity are as we have discussed, a major source of systematic error. Forcing $S(k)$ to unity at large k compensates for this drift as well as the transmission effects discussed above but definitely distorts the large k structure and changes the overall amplitude of $S(k)$ by up to 0.5%. Possibly more important because more difficult to determine, is the angle-dependent distortion of $S(k)$ which will result if the empty cell, neon and helium scans have not seen properly scaled to the same incident intensity; this may amount to perhaps a maximum 2% effect and is to be regarded as a defect in the present work.

TABLE I. Statistical uncertainty in the $S(K)$ measurements introduced by the neon scattering data required for normalization. The predominant statistical error in the data is due to the errors in the neon data.

k (Å^{-1})	$\Delta S(k)$ (%)
0.213	0.2
1.170	0.3
1.851	0.4
2.110	0.5
2.620	0.6
3.653	1.4
4.617	3.1
5.129	4.6

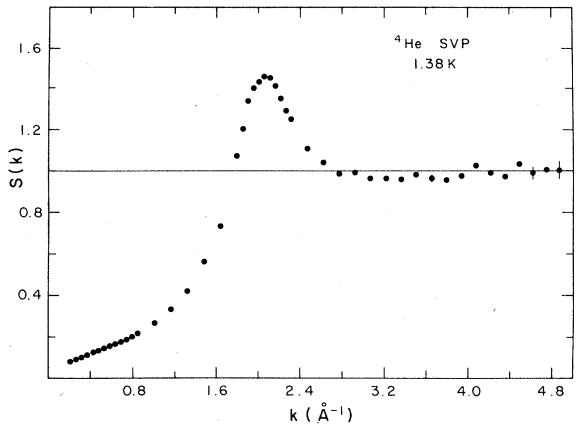

FIG. 2. ^{4}He liquid structure data at 1.38 K. The error bars shown are the statistical errors (1σ) inherent in the scattering data alone and do not include the various possible systematic errors discussed in the text.

The statistical precision of the data is determined at all angles by the neon intensity. Counting statistics for the total counts in four averaged neon scans give (at the level of one standard deviation): 0.3% for $k=0.5$ Å^{-1}, 0.5% for $k=2.1$ Å^{-1}, and 1.4% for $k=3.7$ Å^{-1}. Since $S(k)$ is computed as the difference of two terms [see Eq. (4)], the precision of $S(k)$ is not linear in the statistical precision of the neon density. Table I provides the typical percentage error in $S(k)$ due to neon counting statistics alone for several representative values of momentum transfer. These $\pm 1\sigma$ error bars are plotted for a typical structure factor in Fig. 2; at small k the range of error is smaller than the plotted symbol. These error bars may be taken as representative of the whole range of data reported here.

In an effort to quantify the overall reproducibility of the measurements in the long term, data from ^{4}He at 4.2 K and 2 atm from the very beginning and the very end of the experiments were compared. Both sets of data were reduced in the manner previously described and individual points over the full momentum transfer span never differed by more than 2% and in most cases substantially less than 1%.

Considering the above sources of error, the overall error in the structure factor is determined by the neon statistics and any residual uncompensated intensity offsets. The absolute accuracy may be taken as 4%, however, the relative accuracy of the structure factors within this data set is better, probably 2–3%.

IV. RESULTS

The structure factor of ^{4}He was measured at seven temperatures at saturated vapor pressure: 1.38, 1.67, 2.20, 2.50, 3.00, 3.50, and 4.24 K. The results of these measurements are tabulated in Table II. The data presented in Table II are the result of the analysis presented in the previous section. No smoothing of any kind has been applied to the data. The structure factor at our lowest experimental temperature, 1.38 K, is shown over nearly the full range of experimental momentum transfer values in Fig. 2. Figure 3 shows the full data set in an enlarged scale over the small momentum transfer range. Also shown along the zero momentum transfer axis are the theoretical intercepts[33]

$$S(0)\equiv\lim_{k\to 0}S(k)=\rho k_B T\chi_T=\gamma k_B T/mc^2 \quad . \qquad (6)$$

Here ρ is the density, k_B the Boltzmann constant, χ_T the isothermal compressibility, γ the ratio of specific heats, m the mass of an atom, and c the velocity of ordinary sound in the fluid. The symbols plotted on the axis of Fig. 3 were computed from the right-hand side of Eq. (6) with the known values[22] of γ and c at each temperature. These intercepts provide a test of any structure factor measurement and the present results are consistent with the expected values by smooth extrapolation. It has been argued[33,34] that at small momentum transfer the structure factor should approach the intercept as a quadratic function of k. The present measurements do not extend to small enough values of the momentum transfer to allow an experimental test of this prediction with the present data. A relatively minor modification of the diffractometer will allow a reduction in the minimum attainable momentum transfer to $k\simeq 0.04$ Å^{-1}.

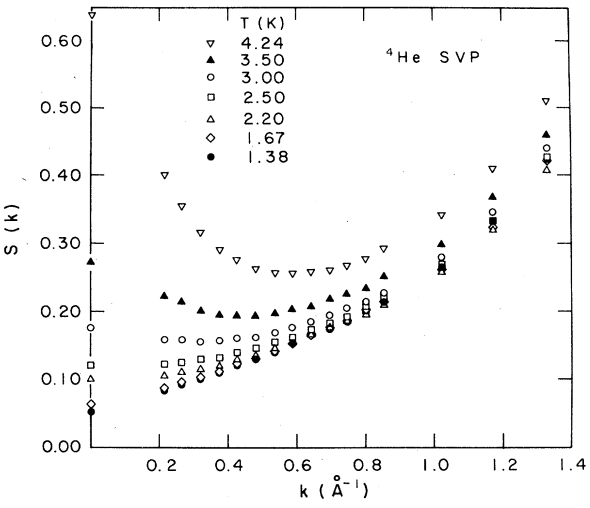

FIG. 3. Small momentum transfer results at saturated vapor pressure for various temperatures. The values plotted at $k=0$ have been computed from thermodynamic data by means of Eq. (6). In all cases the available data are consistent with expectations.

TABLE II. Results for the liquid structure factor of ^{4}He at saturated vapor pressures and several temperatures. The data are shown as obtained from Eq. (4) subject to the corrections discussed in the text. No smoothing has been applied to the data.

	$S(k)$						
k (Å^{-1})	1.30 K	1.67 K	2.20 K	2.50 K	3.00 K	3.50 K	4.24 K
0.213	0.081	0.086	0.106	0.123	0.159	0.222	0.398
0.267	0.091	0.095	0.111	0.125	0.159	0.215	0.355
0.320	0.099	0.102	0.115	0.128	0.154	0.201	0.314
0.373	0.110	0.111	0.120	0.131	0.157	0.194	0.289
0.427	0.122	0.123	0.129	0.139	0.160	0.193	0.274
0.480	0.131	0.131	0.136	0.146	0.162	0.193	0.261
0.533	0.142	0.141	0.144	0.153	0.168	0.197	0.256
0.586	0.154	0.153	0.155	0.161	0.176	0.203	0.256
0.640	0.164	0.162	0.163	0.173	0.185	0.208	0.257
0.693	0.175	0.175	0.174	0.182	0.194	0.218	0.262
0.746	0.186	0.187	0.185	0.192	0.204	0.225	0.267
0.799	0.200	0.201	0.195	0.205	0.213	0.233	0.277
0.852	0.215	0.215	0.210	0.218	0.226	0.249	0.290
1.011	0.265	0.263	0.257	0.269	0.278	0.298	0.341
1.169	0.333	0.323	0.321	0.333	0.345	0.368	0.408
1.328	0.424	0.422	0.408	0.427	0.440	0.459	0.508
1.485	0.563	0.559	0.539	0.555	0.569	0.605	0.651
1.642	0.732	0.770	0.740	0.764	0.783	0.822	0.864
1.799	1.072	1.063	1.060	1.073	1.092	1.075	1.117
1.851	1.201	1.182	1.190	1.212	1.205	1.218	1.219
1.903	1.337	1.346	1.362	1.327	1.327	1.325	1.307
1.955	1.399	1.397	1.435	1.461	1.414	1.396	1.355
2.006	1.433	1.431	1.491	1.491	1.449	1.427	1.363
2.058	1.458	1.449	1.522	1.510	1.477	1.447	1.379
2.109	1.448	1.443	1.489	1.484	1.447	1.433	1.381
2.161	1.412	1.403	1.436	1.424	1.403	1.398	1.346
2.212	1.352	1.342	1.360	1.352	1.330	1.331	1.293
2.264	1.290	1.283	1.290	1.287	1.261	1.264	1.255
2.315	1.249	1.226	1.238	1.234	1.223	1.220	1.215
2.468	1.105	1.098	1.084	1.076	1.069	1.083	1.075
2.620	1.040	1.014	1.011	1.022	1.004	1.018	1.024
2.771	0.986	0.961	0.964	0.964	0.946	0.964	0.977
2.921	0.996		0.963	0.956	0.957	0.984	0.984
3.068	0.964	0.942	0.941	0.967	0.950	0.961	0.960
3.217	0.965	0.945	0.948	0.944	0.947	0.967	0.971
3.364	0.956	0.942	0.943	0.949	0.939	0.953	0.961
3.509	0.980	0.985	0.987	0.983	0.975	0.999	0.998
3.653	0.964	0.980	0.974	0.983	0.973	0.968	1.001
3.795	0.956	0.980	0.958	0.982	0.930	1.010	0.994
3.936	0.974	0.983	0.980	1.010	1.000	1.015	1.041
4.075	1.028	1.051	1.023	1.045	1.043	1.050	1.055
4.213	0.992	0.968	0.956	1.001	0.967	1.010	0.983
4.349	0.973	0.969	0.944	0.984	0.942	0.969	0.989
4.484	1.032	1.037	1.037	1.037	1.048	1.039	1.034
4.617	0.989	0.975	0.992	1.014	0.948	0.987	1.007
4.748	1.005	1.014	1.011	0.959	1.028	0.966	0.987
4.877	1.002	1.066	1.006	1.001	1.034	1.016	1.000
5.004	1.000	0.959	0.963	0.976	0.988	0.986	1.005
5.129	1.007	0.990	1.027	1.047	1.005	1.050	1.006

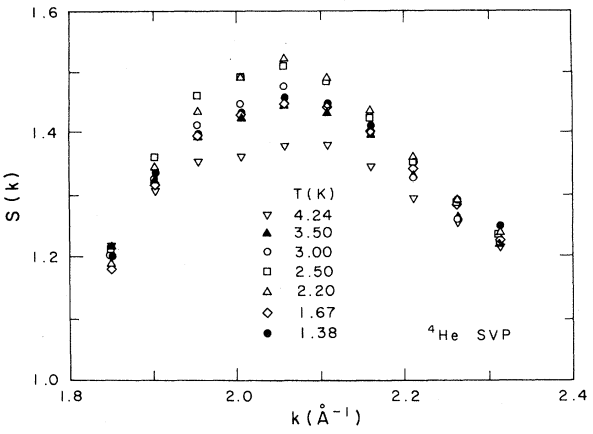

FIG. 4. Evolution of the principal maximum in the structure factor of ^{4}He at saturated vapor pressure as a function of temperature.

Figure 4 illustrates the evolution of the principal maximum of the liquid structure factor at saturated vapor pressure as a function of temperature.

In Fig. 5 is shown the height S_M and position k_m of the principal maximum of the ^{4}He structure factor. Figure 6 illustrates the same data as a function of density; in Fig. 6 the open symbols refer to data obtained below T_λ. The dramatic difference in the amplitude of the principal maximum above and below T_λ is clearly visible. For both Figs. 5 and 6 it is important to keep in mind that all of the data are at saturated vapor pressure. Thus, the data shown in Fig. 6 as a function of density are, of course, at different temperatures.

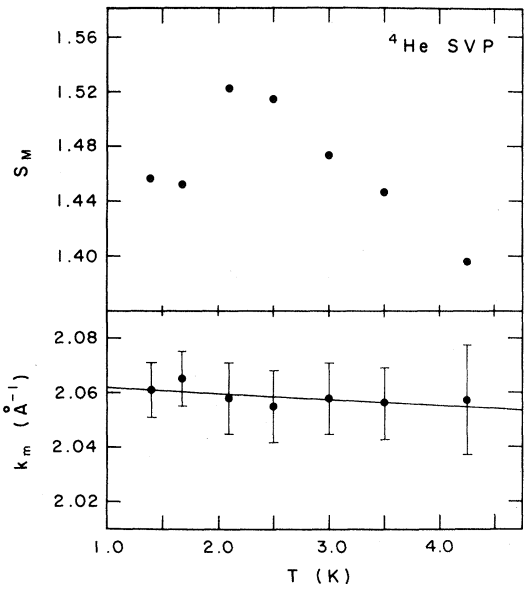

FIG. 5. Amplitude and position of the principal structure factor maximum as a function of temperature. All of the data are at saturated vapor pressure and hence various densities are represented.

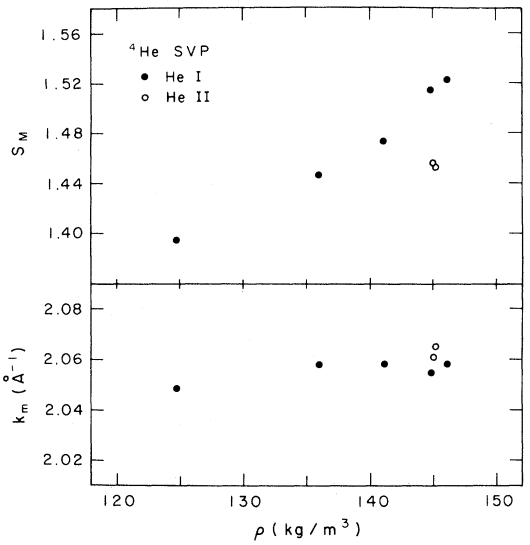

FIG. 6. Amplitude and position of the principal structure factor maximum as a function of density. The open symbols are for temperatures below T_λ.

A comparison between these measurements and those of other workers[13,35–40] is shown in Fig. 7. In Fig. 7 all of the measurements for the peak height, S_M, and its position in momentum transfer, k_m, have been redetermined from the published unsmoothed data wherever possible by the technique of graphical interpolation. We observe considerable spread in the various reported values. In particular, there is an apparent systematic difference between the values of both S_M and k_m between this and the most recent neutron scattering results.[19] In particular, the neutron results for S_M seem to be lower than those we report by the nearly temperature independent factor 0.075. There is also a difference, again independent of temperature, of about 0.015 Å^{-1} in the reported position of the main peak. The source of this disagreement is not understood.

The disagreement between the present results and the recent neutron results of Svensson *et al.*[39,40] is particularly curious since it only is present over a narrow range of momentum transfer values in the immediate vicinity of the principal maximum of the structure factor. This is shown in Fig. 8 where, aside from the region of the peak, the agreement between the very different x-ray and neutron techniques is remarkable. The source of the disparity between the two sets of measurements in the region of the peak is not understood.

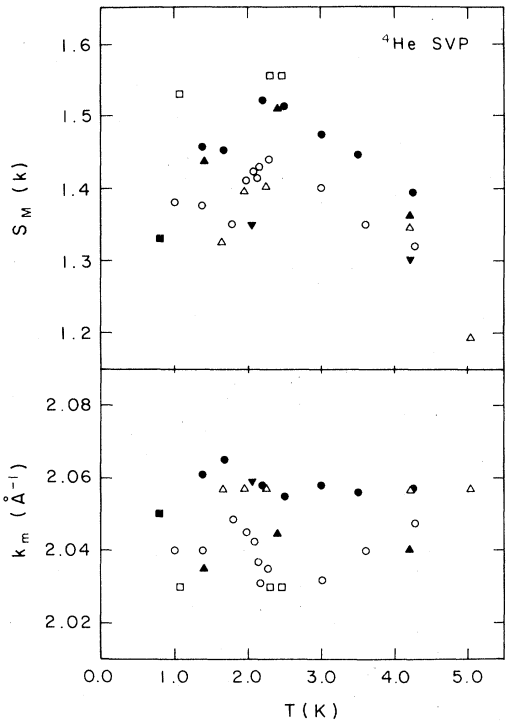

FIG. 7. Comparison of the experimental determination of the height of the principal structure factor peak, S_M, and its position, k_m, at saturated vapor pressure among various experiments. The solid symbols refer to x-ray scattering experiments, the open symbols represent neutron scattering results. The solid dots are for the work we report here, the solid square Ref. 13, the solid triangles Ref. 35, the solid inverted triangles Ref. 36, open circles Ref. 39, open squares Ref. 37, and open triangles Ref. 38.

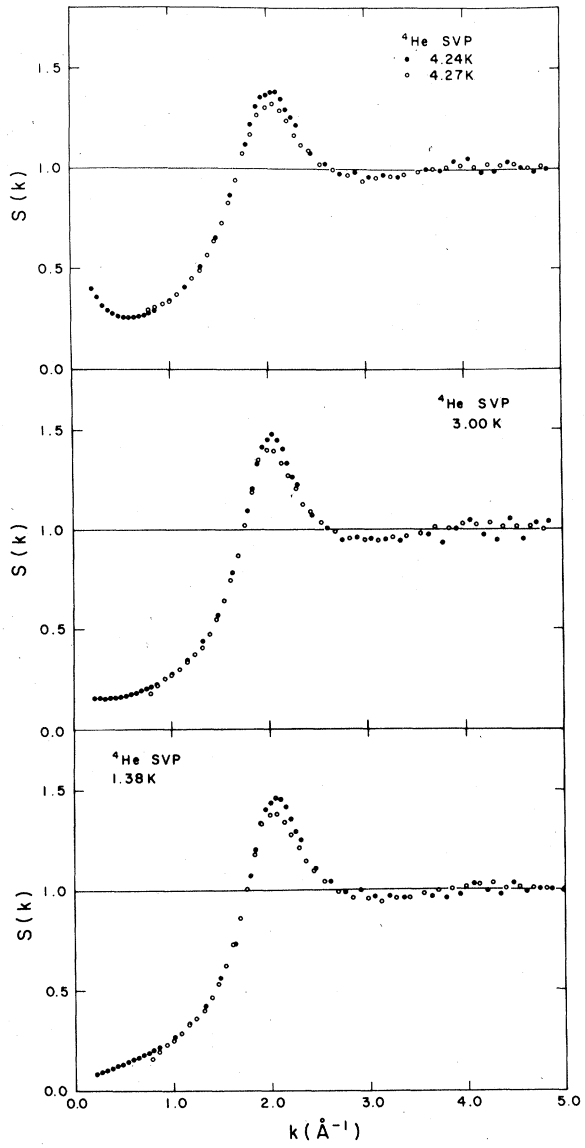

FIG. 8. Comparison between several of the measurements of Svensson *et al.* (Ref. 39) (open circles) and the present work (solid circles). The agreement between the two sets of measurements is remarkable except for a limited region in the vicinity of the principal structure factor peak.

Although not at saturated vapor pressure, the results of Mozer *et al.*[32] can be compared with other measurements[41] we have taken peripheral to the present study. A comparison between our results and those of Mozer *et al.*[32] reveal excellent agreement over a wide range of momentum transfer. For example at $T=2.20$ K and $\rho=0.1618$ kg/m^3 we find $S_M=1.631$ with $k_m=2.090$ Å^{-1} while Mozer finds $S_M=1.619$ and $k_m=2.090$ Å^{-1} at $T=2.86$ K and $\rho=0.1628$ kg/m^3. Given the relative insensitivity of S_M and k_m to changes in temperature above T_λ at fixed density this agreement is quite good.

At small momentum transfer x rays have a distinct advantage over neutrons (the opposite is true for $k \gtrsim 5$ Å^{-1}). In Fig. 9 is shown a comparison between our saturated vapor pressure (SVP) results and those of Svensson *et al.*[39,40] at three temperatures which coincide. Plotted on the $k=0$ axis is the intercept expected on the basis of Eq. (6). The x-ray results have not been smoothed in any way and the scatter in the plotted symbols is indicative of the statistical errors in the small momentum transfer region. By smooth extrapolation the x-ray results are quite consistent with expectations based on Eq. (6). The neutron data represents the average values of $S(k)$ from three adjacent momentum transfer values. The discrepancy between the neutron and x-ray work for $k \lesssim 1$ Å^{-1} is simply indicative of the suitability of the x-ray technique at small k. A similar comparison at $k \gtrsim 5$ Å^{-1} reveals the opposite situation. In that con-

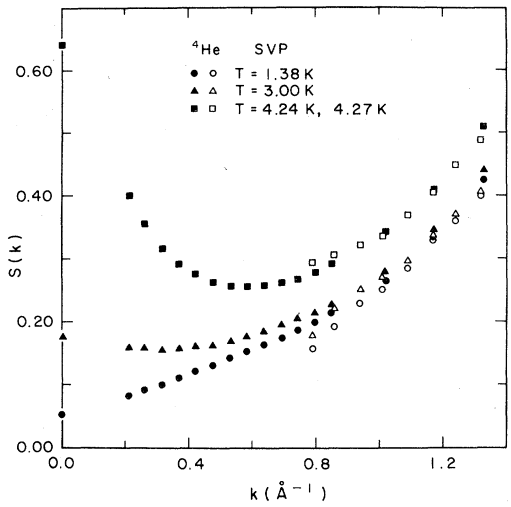

FIG. 9. Comparison between the recent neutron work (Refs. 39 and 40) (open symbols) and the present results (closed symbols) at small momentum transfer.

text the smallness of the helium coherent scattering factor, σ_e, makes it essentially impossible to obtain accurate $S(k)$ data for $k > 5$ Å^{-1}. The neutron scattering technique does not suffer in this way and can be used to good accuracy well beyond $k \simeq 5$ Å^{-1} as shown by the work of Svensson *et al.*[39,40]

Previous x-ray measurements of $S(k)$ by two groups exist but a detailed comparison with the present work is made difficult by the lack of common temperatures. The work of Gordon *et al.*[35] at several similar temperatures is shown in comparison to the present results in Fig. 10. The agreement is good although the present results show evidence for the weak second maximum in the structure factor whereas the results of Gordon *et al.*[35] do not. The differences at small momentum transfer are presumably due to problems with the technique of data analysis used by Gordon *et al.*[35] The results of Achter and Meyer[13] at the considerably lower temperature of 0.79 K are shown in comparison to the present results in Fig. 11. The disagreement at small momentum transfer seen previously[42] is again observed and the disagreement in the momentum transfer interval $1.9 \leq k \leq 4.0$ Å^{-1} is substantial. Previous small momentum transfer structure factor measurements by Hallock[42] are in good agreement with the present results and a comparison between the present work and earlier work is shown in Fig. 12.

Nearly all of the theoretical work on the structure factor has been on the ground state at absolute zero. Finite-temperature efforts are beginning, however, and we will return to discuss them shortly. It is generally acknowledged that the modern era of interest and techniques in the calculation of $S(k)$ began with the

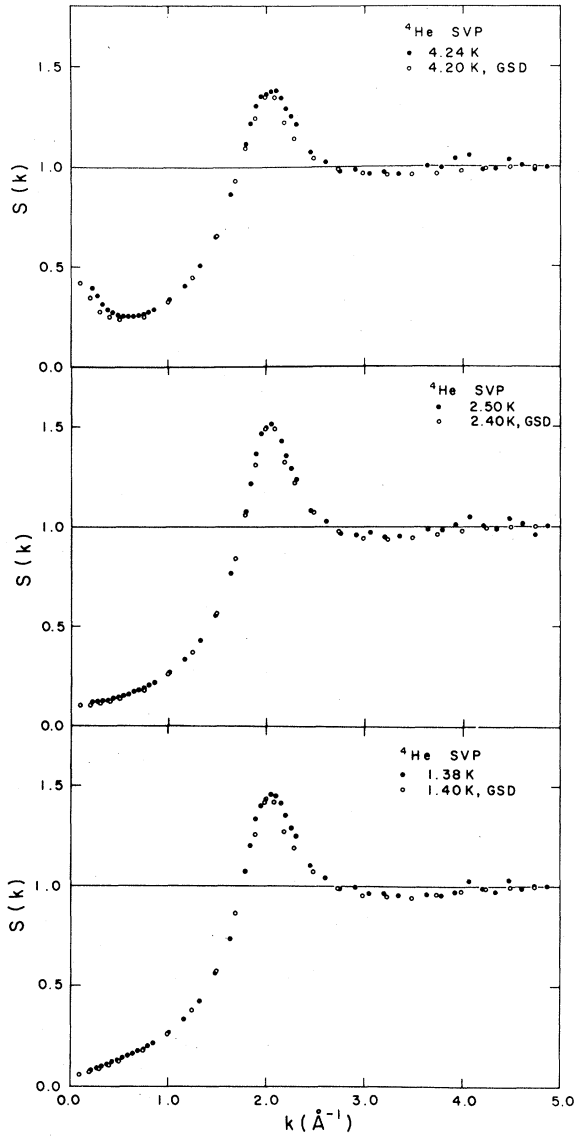

FIG. 10. Comparison between the results of Gordon *et al.* (Ref. 35), GSD, and the present work.

pioneering work of McMillan[43] about 15 years ago. His work consisted of a Monte Carlo calculation based on a wave function made up of the product of pair functions each of which was an exponential in r^{-1}. His and much subsequent work also employed the Lennard-Jones (LJ) 6-12 potential. Such a calculation is also capable of computing the one particle density matrix as a function of r. McMillan[43] found $\rho_1(r) = 0.11\rho$ for $r \gtrsim 4.5$ Å and thus a condensate fraction of 11% at zero temperature resulted from the calculation.

Campbell and Feenberg[44] pointed out that the paired-phonon analysis of Jackson and Feenberg[45]

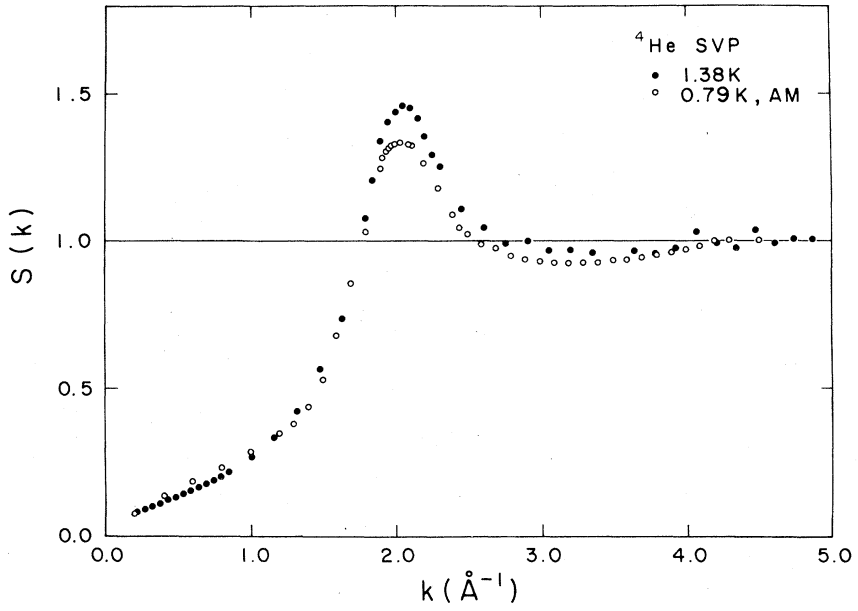

FIG. 11. Comparison between the present work and the results due to Achter and Meyer (Ref. 13) at $T = 0.79$ K.

could in principle be used to obtain the optimal trial function and hence the optimal liquid structure factor could in principal be determined. To carry through the work, however, the hypernetted chain[46] and Percus-Yevick[47] approximation were used in separate calculations. The work was notable in that it was the first to come close to the proper small momentum transfer behavior.

A new integral equation technique was introduced by Francis, Chester, and Reatto[48] along with a pair function chosen to include a long-range term. The addition of the phonon term in the pair function caused a dramatic improvement in the agreement with experimental data at small momentum transfer and a small increase in the amplitude of the computed $S(k)$ in the region of the principal maximum. The work was notable to future progress in that it pointed out a need to incorporate intermediate range

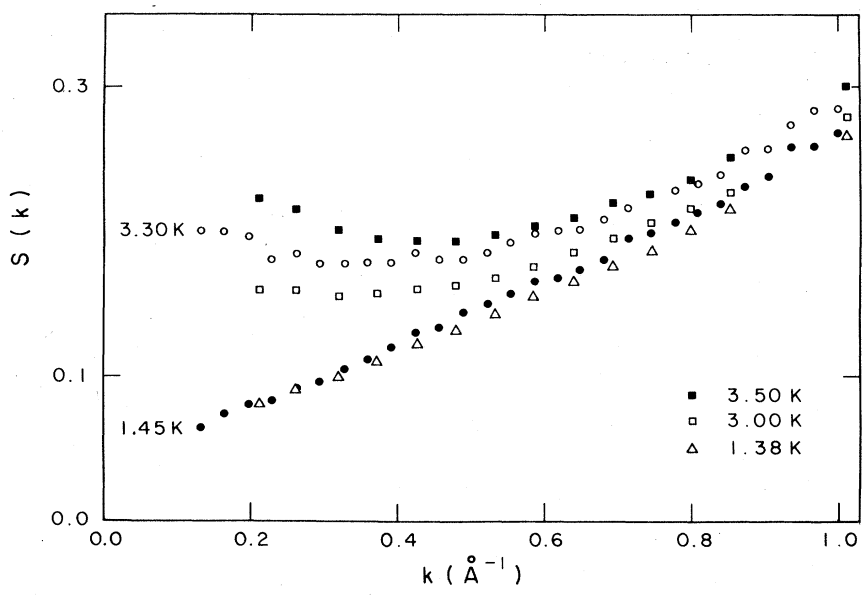

FIG. 12. Results at small momentum transfer in comparison to previous work (open and closed circles) due to Hallock (Ref. 42).

correlations in the pair function. A condensate fraction of 8–10% was found.

A complicated parametrization of the Jastrow function was introduced by De Michelis and Reatto[49] in an effort to introduce attractive correlations. With a LJ 6-12 potential the condensate fraction was observed to be 13% and the agreement between theory and experiment in the case of $S(k)$ was further improved.

The previous few paragraphs are intended to provide the general framework for the most recent theoretical work which we will now discuss and compare with the present experimental results. We will concentrate on three recent developments: the calculations of Chang and Campbell[50] at absolute zero in the paired phonon analysis, the work of Whitlock *et al.*[51] using Monte Carlo techniques, and the work of Reatto[52–54] and his colleagues relevant to the temperature dependence of the liquid structure factor.

In the work of Chang and Campbell[50] the paired-phonon analysis is used to obtain in principle the optimum Jastrow function. A hypernetted-chain approximation is used to obtain the liquid structure factor and it is claimed that the approximation involved in the HNC calculation provides results very close to what would be obtained by Monte Carlo methods. The work consists of essentially four calculations. For each of the LJ 6-12 and the Morse dipole-dipole (MDD2) potentials the problem is formulated once for just two-body factors and again including three-body factors. The use of two potentials showed that the structure factor was most sensitive to the intermediate and long-range behavior[55–57] of the potential. The inclusion of three-body factors resulted in a substantial increase in the calculated amplitude of the principal structure factor peak. In Fig. 13(a) we compare our 1.38-K data with the Chang and Campbell[50] results for the LJ potential for the case of both two-body as well as three-body factors. The improved agreement with experiment in the case of including the three-body factors is evident. Figure 13(b) shows the 1.38-K data in comparison with the theoretical results for the MDD2 as well as the LJ potential. In each case three-body factors have been included in the calculation. The MDD2 three-body calculation is in rather close agreement with the experimental results. This provides experimental verification that the presence of three-body effects in such calculations is crucial as is the choice of the potential used.

Quite recently Whitlock *et al.*[51] have used the Green's function Monte Carlo[58] method within the context of the LJ 6-12 potential in an extensive study of ^{4}He as a function of density. Their work at equilibrium density shows more structure in the liquid structure factor principal maximum than previous Monte Carlo calculations and verifies the importance of three-body correlations emphasized by Chang and Campbell.[50] The Monte Carlo results are

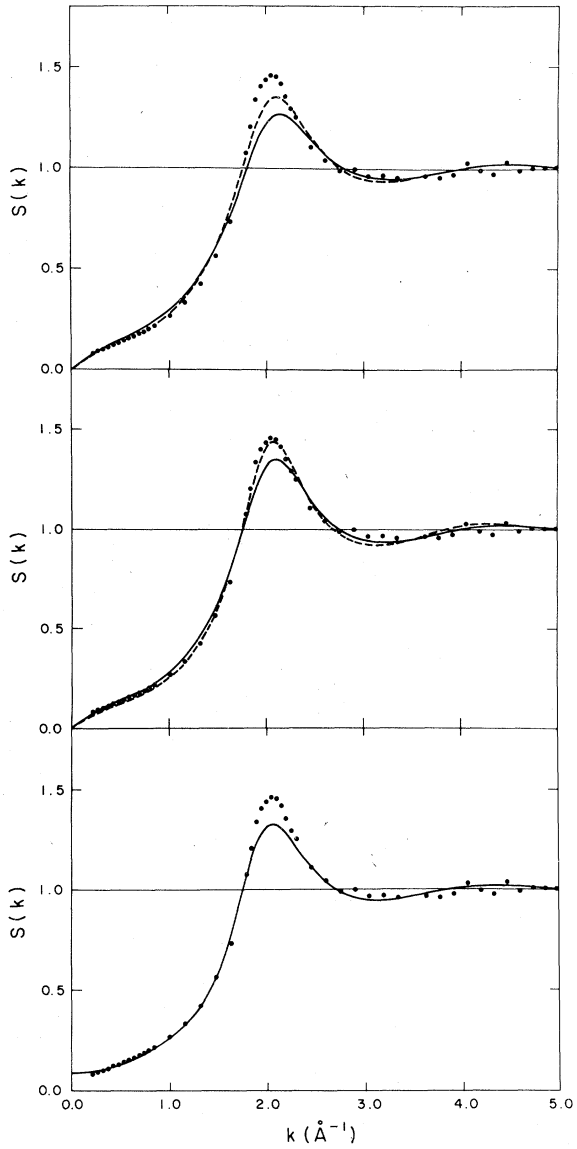

FIG. 13. Comparison of the present raw liquid structure factor data at $T = 1.38$ K with the calculations of: (a) Chang and Campbell (Ref. 50) for the Leonnard-Jones potential in the case of two-body (——) and three-body (– – –) factors; (b) Chang and Campbell (Ref. 50) for three-body factors in the case of the Leonnard-Jones (——) and MDD2 (– – –) potentials; and (c) Whitlock *et al.* (Ref. 51) for the Leonnard-Jones potential.

in some sense exact for a given choice of potential and a comparison is made between the work of Whitlock *et al.*[51] and our saturated vapor pressure data at 1.38 K in Fig. 13(c). The comparison suggests that the LJ potential is not the best choice for the description of ^{4}He from the point of view of the liquid structure factor. The Chang and Campbell[50] MDD2 three-body calculation is much closer to the

experimental observations which suggests the MDD2 may be more appropriate for studies of the structure of helium than is the LJ potential. The results of this calculation yield a condensate fraction of 11.2% at saturated vapor pressure with a decrease observed for increasing density.

Of particular interest is the behavior of the structure factor in the vicinity of the λ transition. Over the years there has been growing evidence that the amplitude of the principal structure factor maximum illustrates a decrease as a function of decreasing temperature.[32,35,37,38] This is shown for the present work in Fig. 5 and in a somewhat different representation in Fig. 6. Since the data for $T \leq 2.5$ K are all at essentially the same density it is clear that the presence of the λ transition has a visible and in fact a dramatic effect on the temperature evolution of the structure factor. The reason for this is presently the subject of debate. Cummings *et al.*[59,60] have suggested that such data may be used to determine the condensate fraction in ^{4}He. From this point of view the loss in spatial order in the superfluid is a direct result of the formation of a Bose condensate of macroscopic occupation. Indeed, x-ray results at both saturated vapor pressure and constant density[61] and neutron scattering results[62] at saturated vapor pressure have recently been analyzed from the point of view of Cummings *et al.*[59,60] with numerical results rather consistent with expectations.

The proposal of Cummings *et al.*[59,60] is however subject to criticism. Fetter[63] has shown that the factorization $n_0 = f(r)h(T)$ which results from the theory when Bose condensation is present is not a feature of all systems which display a Bose condensation. In particular, he cites a counterexample. Griffin[64] has shown recently that terms neglected in the analysis of Cummings *et al.*[59,60] may be at least as important as those retained and hence questions, among other things, the validity of numerical results based on their prescription.

Reatto and his co-workers have developed an alternate approach to the interpretation of the fact that the observed spatial order in ^{4}He decreases with a decrease in temperature below T_λ. Their work was based on a calculation[53] which considered a wide class of trial functions with the conclusion that better agreement with experiment from the point of view of $S(k)$ could be obtained if a repulsive structure existed centered between the first and second peaks of the pair correlation function. This structure was interpreted as being due to the zero point motion of rotons. Within the context of the Penrose density matrix it was shown[52] that there is an enhancement of this short-range spatial order with an increase in temperature. The interpretation is that this is due to the thermal excitation of rotons. Thus, from this point of view an increase in temperature from absolute zero should result in an increase in the spatial structure of liquid ^{4}He—precisely the qualitative behavior observed in recent experiments.

The results of the temperature-dependent calculation of De Michelis *et al.*[52] are shown in Fig. 14 along with data from the present experiments. Shown is the difference between the structure factor values at 2.20 and 1.38 K as determined experimentally. The dashed line drawn through the data is merely a guide to the eye. The solid line represents the theoretical prediction for the difference $\Delta = (S(k, T = T_\lambda) - S(k, T = 0)$ at the equilibrium density. There is clear qualitative agreement although the difference function is observed to be substantially sharper in the experiments.

Recently Reatto and co-workers[54] have completed a Monte Carlo study of the LJ system with a correlation structure (such as we have described) in the Jastrow function. The previous conclusions concerning an increase in $S(k)$ with temperature are confirmed for the LJ system. Although not optimized, a density-dependent study was carried out with the conclusion that the intermediate structure increases in strength with density. Thus, density-dependent experiments on the spatial order at and below T_λ should allow one to comment on the relevance of the Cummings explanation versus that proposed by Reatto and co-workers.

The data obtained in these measurements cover an adequate range of momentum transfer to allow a Fourier transform of reasonable accuracy so as to obtain the pair correlation function $g(r)$. To accomplish this transformation a smooth curve was drawn through the data points and the smoothed data set $S_s(k)$ (Table III) was enhanced in density and made equally spaced in momentum transfer by a scheme of

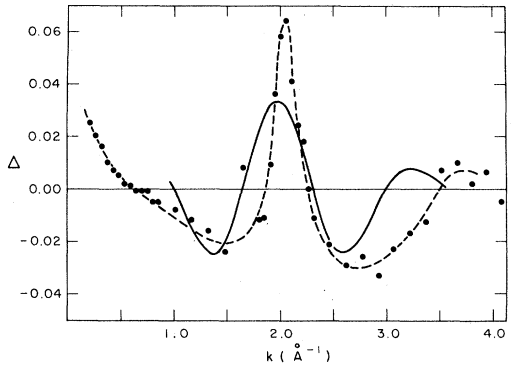

FIG. 14. The difference between the liquid structure factor at or near T_λ and that obtained at a much lower temperature. The data points represent $\Delta = S(k, T = 2.20$ K$) - S(k, T = 1.38$ K$)$ as determined in the present work at saturated vapor pressure. The dashed line is a guide to the eye only. The solid line represents the theoretical work of Ref. 52 for $\Delta = S(k, T = T_\lambda) - S(k, T = 0)$.

TABLE III. Smoothed liquid structure values for ^{4}He at saturated vapor pressure, $S_S(k)$.

k (Å^{-1})	1.38 K	1.67 K	2.20 K	2.50 K	3.00 K	3.50 K	4.24 K
0.000	0.051	0.064	0.100	0.121	0.176	0.272	0.640
0.100	0.062	0.072	0.101	0.117	0.167	0.248	0.524
0.200	0.077	0.084	0.106	0.119	0.153	0.225	0.407
0.299	0.094	0.099	0.114	0.125	0.154	0.206	0.332
0.399	0.114	0.116	0.123	0.134	0.154	0.193	0.281
0.499	0.133	0.134	0.138	0.147	0.163	0.193	0.259
0.599	0.155	0.155	0.156	0.164	0.177	0.202	0.256
0.699	0.177	0.175	0.175	0.181	0.193	0.215	0.260
0.798	0.199	0.200	0.200	0.202	0.212	0.234	0.278
0.898	0.229	0.231	0.226	0.230	0.236	0.259	0.303
0.998	0.261	0.262	0.256	0.264	0.273	0.294	0.338
1.098	0.303	0.300	0.292	0.303	0.315	0.334	0.378
1.198	0.348	0.346	0.335	0.350	0.363	0.383	0.424
1.297	0.404	0.406	0.394	0.411	0.420	0.439	0.481
1.397	0.484	0.477	0.462	0.482	0.490	0.519	0.566
1.497	0.579	0.578	0.558	0.573	0.590	0.625	0.668
1.597	0.691	0.702	0.682	0.699	0.720	0.748	0.802
1.697	0.831	0.864	0.848	0.874	0.878	0.913	0.951
1.796	1.075	1.065	1.060	1.087	1.087	1.083	1.122
1.896	1.313	1.300	1.323	1.349	1.310	1.304	1.297
1.996	1.432	1.432	1.484	1.492	1.452	1.429	1.374
2.096	1.450	1.447	1.503	1.495	1.459	1.440	1.383
2.196	1.369	1.354	1.383	1.373	1.356	1.357	1.314
2.295	1.255	1.247	1.250	1.253	1.232	1.234	1.229
2.395	1.166	1.150	1.148	1.144	1.132	1.147	1.149
2.495	1.089	1.080	1.069	1.064	1.054	1.071	1.075
2.595	1.041	1.028	1.019	1.016	1.005	1.021	1.030
2.695	1.013	0.990	0.986	0.991	0.978	0.995	1.001
2.794	0.995	0.966	0.968	0.976	0.960	0.981	0.985
2.894	0.983	0.955	0.953	0.966	0.950	0.971	0.973
2.994	0.974	0.949	0.951	0.960	0.947	0.971	0.970
3.094	0.967	0.946	0.947	0.957	0.945	0.967	0.968
3.194	0.963	0.947	0.951	0.955	0.942	0.967	0.968
3.293	0.962	0.947	0.950	0.957	0.947	0.967	0.970
3.393	0.961	0.952	0.952	0.959	0.948	0.969	0.976
3.493	0.962	0.959	0.954	0.963	0.949	0.972	0.982
3.593	0.964	0.967	0.958	0.968	0.954	0.979	0.987
3.693	0.966	0.976	0.964	0.974	0.961	0.986	0.994
3.792	0.972	0.986	0.971	0.985	0.968	0.994	1.001
3.892	0.982	0.996	0.978	0.994	0.977	1.002	1.010
3.992	0.989	1.006	0.983	1.002	0.989	1.009	1.017
4.092	0.999	1.011	0.993	1.003	1.001	1.013	1.020
4.192	1.005	1.017	1.003	1.013	1.008	1.017	1.023
4.291	1.009	1.020	1.006	1.016	1.014	1.017	1.022
4.391	1.014	1.022	1.013	1.016	1.018	1.021	1.019
4.491	1.014	1.022	1.014	1.017	1.019	1.021	1.018
4.591	1.016	1.020	1.014	1.014	1.022	1.021	1.014
4.691	1.013	1.019	1.014	1.012	1.018	1.016	1.006
4.790	1.009	1.014	1.009	1.008	1.015	1.008	1.001
4.890	1.004	1.010	1.004	1.002	1.006	1.003	1.001

Lagrangian interpolation. During this procedure the original data set was extended smoothly to the intercept at $k=0$ obtained from Eq. (6). An example of a pair correlation function obtained by this procedure is shown in Fig. 15 for the case of 1.38 K.

In Fig. 16 comparison is made to the recent neutron scattering determinations of $g(r)$ by Sears *et al.*[39] as well as to theoretical predictions.[50,51] In each case in Fig. 16 the smooth curve is the pair correlation function at 1.38 K as determined (Table IV) from the present measurements. In comparison to the neutron results the present work shows a principal $g(r)$ peak slightly lower and shifted to smaller coordinate. The largest difference between the two measurements is found in the vicinity of the first minimum. The $T=0$ theoretical results of Chang and Campbell[50] [Fig. 16(b)] for the case of the MDD2 potential predict a principal maximum more narrow than seen experimentally in either these measurements or those of Sears *et al.*[39] The location of the principal maximum is also displaced in the theory. The Monte Carlo results of Whitlock *et al.*[51] for the case of the Leonnard-Jones potential are shown in Fig. 16(c). The calculation predicts slightly less structure than seen in either these or the neutron measurements.[39]

In the display of our experimental results for the pair correlation function we have truncated the Fourier transform for values of the coordinate smaller than r_c where $g(r)$ reaches zero due to the hard core of the atom. An additional transform of the so truncated $g(r)$ can be carried out to obtain a liquid structure factor which can be compared with the original experimental structure factor. We call this new structure factor $S_T(k)$ to indicate that it has been obtained from the modified pair correlation function by

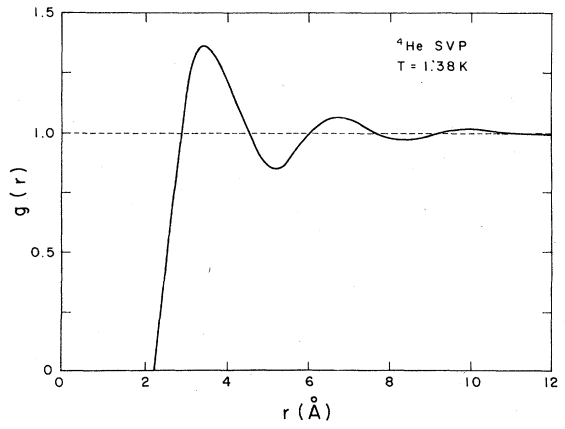

FIG. 15. The pair correlation function, $g(r)$, for $T=1.38$ K as determined from the smoothed liquid structure factor, $S_S(k)$, is given in Table III. Numerical values for this and other temperatures appear in Table IV.

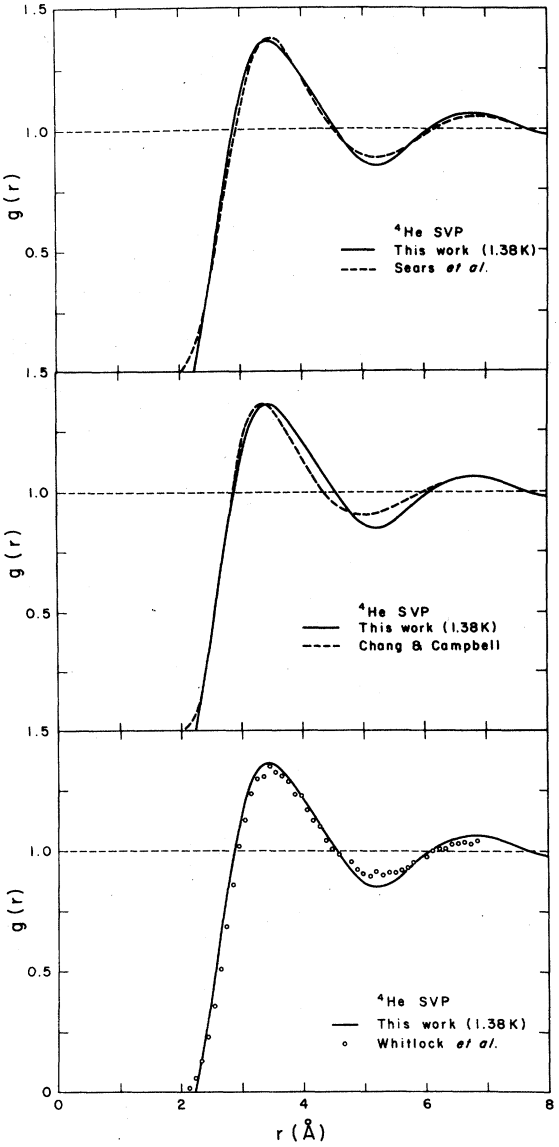

FIG. 16. Comparison between the pair correlation function determined in this work and that found by (a) Sears *et al.* (Ref. 39) and determined theoretically by (b) Chang and Campbell (Ref. 50) (three-body, MDD2 potential), and (c) Whitlock *et al.* (Ref. 51).

a Fourier transform. Comparison is made between $S_T(k)$ and the smoothed measured structure factor, $S_S(k)$ in Fig. 17. In general the $S_T(k)$ values so obtained are lower in the region of the principal maximum that are the directly determined $S(k)$ values. This is observed to be true at all temperatures. The oscillations at small momentum transfer seen in $S_T(k)$ are due to the truncation of $g(r)$ beyond $r \cong 12$ Å.

TABLE IV. Values of the pair correlation function for ^{4}He at saturated vapor pressure as determined from the structure factor data presented in Table III.

	$g(r)$						
r (Å)	1.38 K	1.67 K	2.20 K	2.50 K	3.00 K	3.50 K	4.24 K
2.212	0.000	0.000	0.000	0.000	0.000	0.000	0.000
2.312	0.065	0.054	0.043	0.052	0.031	0.001	0.061
2.413	0.186	0.152	0.149	0.151	0.123	0.092	0.149
2.513	0.345	0.293	0.301	0.291	0.268	0.239	0.273
2.614	0.517	0.459	0.476	0.452	0.444	0.419	0.417
2.714	0.685	0.632	0.651	0.619	0.626	0.606	0.572
2.815	0.842	0.800	0.814	0.780	0.798	0.783	0.730
2.915	0.985	0.956	0.964	0.931	0.954	0.943	0.885
3.016	1.109	1.095	1.096	1.068	1.090	1.083	1.029
3.116	1.208	1.209	1.204	1.183	1.201	1.198	1.154
3.217	1.278	1.292	1.284	1.270	1.282	1.282	1.252
3.318	1.320	1.343	1.335	1.329	1.332	1.334	1.323
3.418	1.340	1.368	1.361	1.362	1.354	1.358	1.365
3.519	1.343	1.371	1.369	1.373	1.358	1.363	1.383
3.619	1.331	1.357	1.361	1.367	1.347	1.353	1.379
3.720	1.308	1.330	1.341	1.346	1.327	1.333	1.357
3.820	1.277	1.294	1.312	1.315	1.298	1.305	1.322
3.921	1.243	1.255	1.277	1.278	1.265	1.273	1.280
4.021	1.208	1.214	1.239	1.237	1.232	1.239	1.235
4.122	1.173	1.173	1.199	1.196	1.198	1.205	1.191
4.222	1.136	1.132	1.157	1.154	1.162	1.170	1.148
4.323	1.098	1.091	1.114	1.111	1.124	1.131	1.107
4.423	1.059	1.051	1.068	1.069	1.082	1.090	1.070
4.524	1.021	1.013	1.024	1.028	1.040	1.047	1.036
4.624	0.984	0.976	0.981	0.989	0.998	1.004	1.004
4.725	0.949	0.942	0.941	0.952	0.958	0.963	0.975
4.825	0.917	0.913	0.904	0.919	0.920	0.924	0.948
4.926	0.890	0.888	0.874	0.890	0.887	0.891	0.924
5.027	0.870	0.871	0.852	0.868	0.863	0.865	0.905
5.127	0.858	0.861	0.840	0.853	0.848	0.850	0.892
5.228	0.854	0.859	0.837	0.847	0.843	0.844	0.883
5.328	0.857	0.864	0.841	0.847	0.846	0.847	0.881
5.429	0.867	0.874	0.854	0.855	0.857	0.858	0.886
5.529	0.883	0.889	0.872	0.869	0.875	0.876	0.896
5.630	0.904	0.908	0.895	0.889	0.897	0.898	0.911
5.730	0.926	0.928	0.920	0.911	0.921	0.923	0.929
5.831	0.948	0.949	0.945	0.935	0.946	0.947	0.949
5.931	0.970	0.968	0.968	0.959	0.968	0.969	0.969
6.032	0.991	0.986	0.990	0.982	0.989	0.990	0.988
6.132	1.009	1.003	1.010	1.003	1.007	1.008	1.005
6.233	1.024	1.018	1.026	1.021	1.023	1.023	1.019
6.333	1.036	1.030	1.039	1.037	1.035	1.036	1.030
6.434	1.045	1.041	1.049	1.049	1.045	1.045	1.038
6.535	1.052	1.049	1.057	1.058	1.053	1.053	1.044
6.635	1.057	1.055	1.063	1.064	1.059	1.058	1.047
6.736	1.059	1.058	1.066	1.068	1.062	1.062	1.048
6.836	1.059	1.058	1.066	1.068	1.063	1.062	1.047
6.937	1.056	1.056	1.064	1.066	1.061	1.061	1.046
7.037	1.052	1.051	1.060	1.061	1.057	1.056	1.043
7.138	1.046	1.045	1.053	1.054	1.051	1.050	1.039
7.238	1.039	1.037	1.045	1.045	1.043	1.042	1.034
7.339	1.030	1.027	1.035	1.036	1.033	1.032	1.028
7.439	1.020	1.018	1.024	1.025	1.023	1.021	1.021
7.540	1.011	1.009	1.013	1.014	1.012	1.010	1.015
7.640	1.001	1.000	1.003	1.004	1.002	1.001	1.008
7.741	0.993	0.993	0.993	0.994	0.993	0.992	1.001
7.841	0.986	0.988	0.985	0.986	0.986	0.985	0.995

TABLE IV (*Continued*).

				$g(r)$			
r (Å)	1.38 K	1.67 K	2.20 K	2.50 K	3.00 K	3.50 K	4.24 K
8.042	0.976	0.980	0.973	0.974	0.976	0.976	0.987
8.143	0.973	0.978	0.970	0.971	0.974	0.974	0.984
8.244	0.972	0.977	0.968	0.969	0.973	0.974	0.983
8.344	0.972	0.977	0.968	0.969	0.973	0.974	0.984
8.445	0.972	0.977	0.969	0.969	0.973	0.975	0.985
8.545	0.974	0.978	0.971	0.971	0.974	0.976	0.986
8.646	0.976	0.979	0.973	0.974	0.976	0.978	0.988
8.746	0.979	0.981	0.977	0.977	0.979	0.981	0.990
8.847	0.983	0.984	0.981	0.981	0.982	0.984	0.993
8.947	0.987	0.987	0.985	0.985	0.986	0.988	0.995
9.048	0.991	0.991	0.990	0.990	0.990	0.992	0.997
9.148	0.996	0.995	0.995	0.995	0.995	0.997	0.999
9.249	1.000	0.999	1.000	0.999	1.000	1.002	1.001
9.349	1.004	1.003	1.005	1.004	1.004	1.007	1.003
9.450	1.008	1.007	1.009	1.008	1.008	1.010	1.004
9.550	1.011	1.009	1.013	1.011	1.012	1.013	1.006
9.651	1.013	1.011	1.016	1.014	1.014	1.016	1.008
9.752	1.014	1.013	1.017	1.016	1.015	1.017	1.009
9.852	1.015	1.013	1.018	1.016	1.016	1.016	1.009
9.953	1.015	1.013	1.018	1.016	1.015	1.015	1.009
10.053	1.014	1.012	1.017	1.015	1.013	1.013	1.009
10.154	1.012	1.011	1.015	1.013	1.011	1.011	1.008
10.254	1.010	1.009	1.013	1.011	1.009	1.009	1.006
10.355	1.008	1.008	1.011	1.009	1.007	1.006	1.005
10.455	1.006	1.006	1.008	1.007	1.005	1.004	1.003
10.556	1.005	1.005	1.005	1.005	1.003	1.002	1.002
10.656	1.003	1.003	1.003	1.003	1.002	1.000	1.000
10.757	1.001	1.002	1.000	1.001	1.001	0.999	1.000
10.857	1.000	1.000	0.998	0.999	0.999	0.998	0.999
10.958	0.998	0.998	0.996	0.997	0.998	0.996	0.999
11.058	0.997	0.996	0.994	0.996	0.997	0.995	0.998
11.159	0.996	0.995	0.992	0.995	0.995	0.994	0.998
11.259	0.995	0.994	0.991	0.994	0.994	0.993	0.998
11.360	0.993	0.993	0.990	0.993	0.993	0.992	0.998
11.461	0.993	0.992	0.990	0.992	0.992	0.991	0.998
11.561	0.992	0.992	0.990	0.992	0.992	0.991	0.998
11.662	0.992	0.993	0.991	0.993	0.993	0.992	0.998
11.762	0.993	0.994	0.992	0.993	0.994	0.993	0.998
11.863	0.993	0.995	0.994	0.995	0.995	0.995	0.998
11.963	0.994	0.996	0.996	0.996	0.996	0.997	0.998
12.064	0.996	0.998	0.998	0.997	0.998	0.999	0.999
12.164	0.997	0.999	1.000	0.999	1.000	1.001	0.999
12.265	0.998	1.001	1.002	1.000	1.002	1.003	1.000
12.365	1.000	1.002	1.004	1.002	1.003	1.005	1.001
12.466	1.001	1.003	1.004	1.003	1.004	1.005	1.002
12.566	1.002	1.003	1.005	1.003	1.004	1.005	1.002

This process can be repeated with little subsequent change in the structure factor values obtained. That is, $S_T(k)$ is corrected at small momentum transfer by use of $S_S(k)$ and a second transform done to get $g_2(r)$ (which is again truncated below r_c) and then $S_{T2}(k)$. The effect of such a process is to restore most of the amplitude lost by $S_T(k)$ in the vicinity of $k = 1.5$ Å^{-1}. The process does not restore the peak amplitude values seen in the original data; there is little change in the principal maximum between $S_T(k)$ and $S_{T2}(k)$. A comparison between $S_{T2}(k)$ (Table V) the liquid in Fig. 18. A further comparison is shown in Fig. 19 where $S_{T2}(k)$ is shown in the region of the principal structure factor maximum

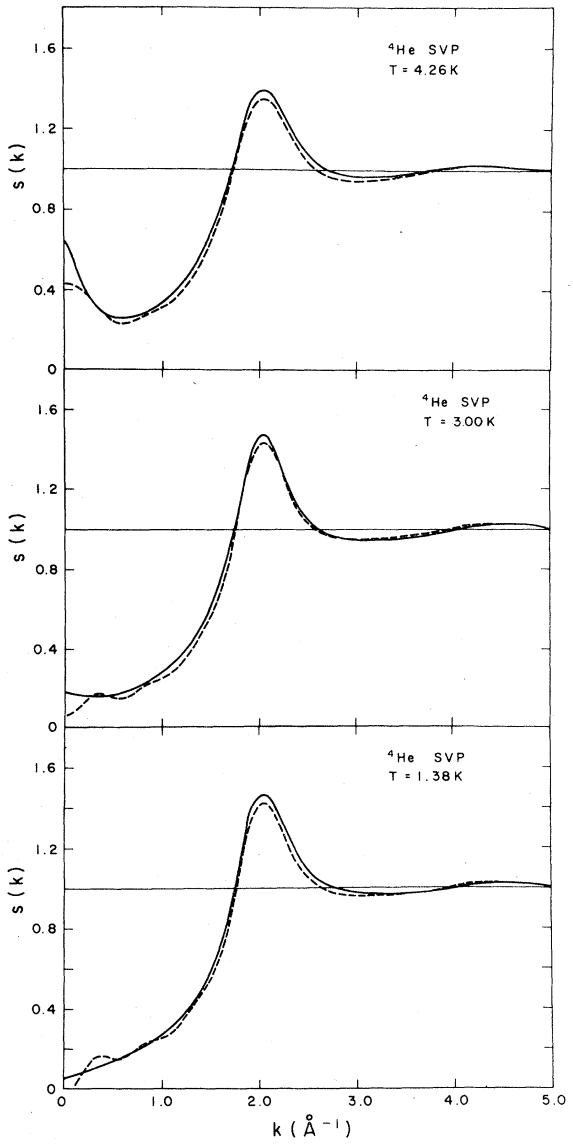

FIG. 17. Illustration of the liquid structure factor, $S_T(k)$, obtained (– – –) after once transforming to obtain $g(r)$ as described in the text. The solid curve is the smoothed structure factor $S_S(k)$.

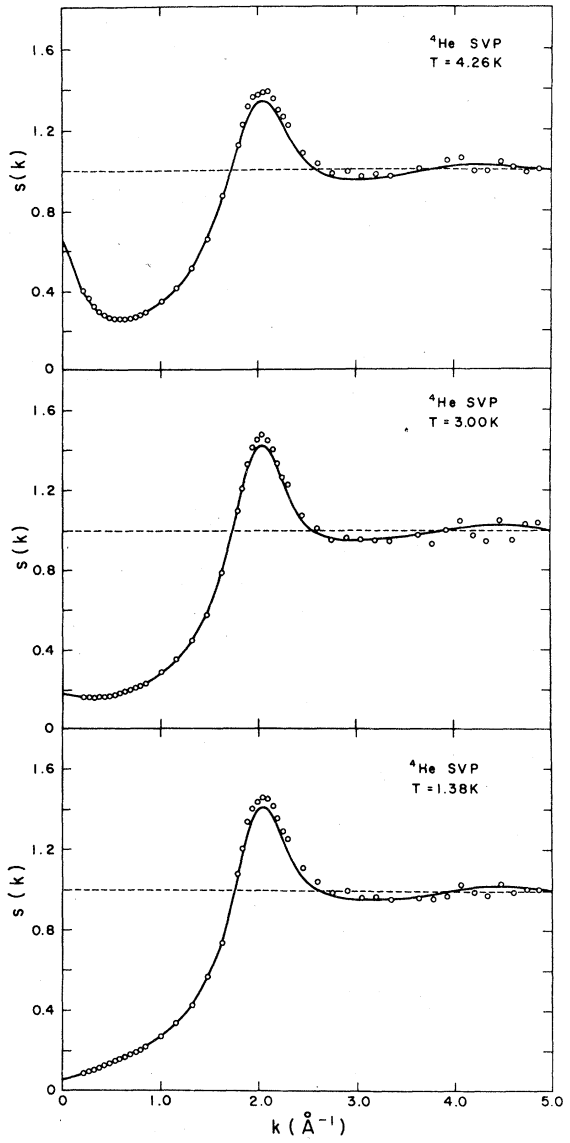

FIG. 18. Comparison between $S_{T2}(k)$(——) and the original structure factor data obtained in this work. As discussed in the text, the data below $k \simeq 1$ Å^{-1} are obtained from $S_S(k)$ to avoid the spurious oscillations at small k introduced by the Fourier transform.

along with both the experimental data from this work as well as that from the work of Sears *et al.* A final comparison is shown in Figs. 20 and 21 where the structure factor $S_{T2}(k)$ is shown with the three-body calculations of Chang and Campbell[50] and the Monte Carlo calculations of Whitlock *et al.*[51]

A consistency relation exists which must be satisfied by a *perfect* liquid structure factor. That is, the sum rule

$$I = \frac{1}{2\pi^2\rho}\int_0^\infty [S(k)-1]k^2dk = -1 \qquad (7)$$

should be exactly satisfied for the perfect structure factor. We have applied this integral condition to the various structure factors discussed here and the results are shown in Table VI. Caution must be emphasized in the use of Eq. (7) due to the sensitivity

TABLE V. Values for the liquid structure factor, $S_{T2}(k)$, for ^{4}He at saturated vapor pressure. These values, as discussed in the text, result from two successive determinations of the pair correlation function.

k (Å)	1.38 K	1.67 K	2.20 K	2.50 K	3.00 K	3.50 K	4.24 K
0.000	0.051	0.064	0.100	0.121	0.176	0.272	0.640
0.100	0.062	0.072	0.101	0.101	0.167	0.248	0.524
0.200	0.077	0.084	0.106	0.106	0.158	0.225	0.407
0.299	0.094	0.099	0.114	0.114	0.154	0.206	0.332
0.399	0.114	0.116	0.123	0.123	0.154	0.193	0.281
0.499	0.133	0.134	0.138	0.138	0.163	0.193	0.259
0.599	0.155	0.155	0.156	0.156	0.177	0.202	0.256
0.699	0.177	0.175	0.175	0.175	0.193	0.215	0.260
0.798	0.199	0.200	0.200	0.200	0.212	0.234	0.278
0.898	0.229	0.231	0.226	0.226	0.236	0.259	0.303
0.998	0.261	0.262	0.256	0.256	0.273	0.294	0.338
1.098	0.303	0.300	0.292	0.292	0.315	0.334	0.378
1.198	0.348	0.346	0.335	0.335	0.363	0.383	0.424
1.297	0.404	0.406	0.394	0.394	0.420	0.439	0.481
1.397	0.484	0.477	0.462	0.462	0.490	0.519	0.566
1.497	0.579	0.578	0.558	0.588	0.590	0.625	0.668
1.597	0.691	0.702	0.682	0.682	0.720	0.748	0.802
1.697	0.831	0.850	0.826	0.848	0.861	0.878	0.929
1.796	1.040	1.057	1.049	1.070	1.069	1.071	1.092
1.896	1.246	1.255	1.272	1.284	1.268	1.260	1.233
1.996	1.978	1.383	1.420	1.418	1.395	1.385	1.318
2.096	1.400	1.405	1.445	1.433	1.414	1.406	1.329
2.196	1.327	1.336	1.357	1.344	1.335	1.330	1.275
2.295	1.214	1.224	1.221	1.212	1.211	1.207	1.188
2.395	1.113	1.121	1.102	1.096	1.100	1.095	1.101
2.495	1.045	1.051	1.030	1.023	1.028	1.023	1.036
2.595	1.007	1.009	0.995	0.988	0.991	0.987	0.994
2.695	0.983	0.979	0.973	0.968	0.970	0.968	0.970
2.794	0.965	0.956	0.953	0.954	0.955	0.953	0.955
2.894	0.955	0.941	0.939	0.945	0.945	0.943	0.946
2.994	0.952	0.938	0.938	0.943	0.945	0.943	0.944
3.094	0.953	0.942	0.947	0.947	0.950	0.949	0.946
3.194	0.954	0.946	0.954	0.951	0.954	0.955	0.950
3.293	0.954	0.947	0.957	0.953	0.956	0.957	0.955
3.393	0.956	0.950	0.957	0.955	0.957	0.958	0.961
3.493	0.961	0.957	0.962	0.961	0.962	0.962	0.969
3.593	0.967	0.969	0.971	0.971	0.969	0.970	0.978
3.693	0.973	0.980	0.980	0.981	0.976	0.978	0.987
3.792	0.979	0.990	0.986	0.989	0.983	0.984	0.996
3.892	0.988	0.998	0.991	0.997	0.990	0.992	1.005
3.992	0.999	1.007	0.999	1.007	1.001	1.001	1.012
4.092	1.009	1.015	1.008	1.015	1.011	1.012	1.017
4.192	1.016	1.020	1.017	1.020	1.019	1.020	1.020
4.291	1.019	1.021	1.021	1.021	1.022	1.023	1.020
4.391	1.021	1.021	1.022	1.020	1.023	1.024	1.018
4.491	1.022	1.020	1.022	1.019	1.024	1.024	1.016
4.591	1.021	1.020	1.022	1.017	1.025	1.025	1.011
4.691	1.018	1.017	1.019	1.014	1.021	1.022	1.006
4.790	1.012	1.012	1.012	1.008	1.014	1.014	1.000
4.890	1.006	1.005	1.005	1.002	1.004	1.004	0.997

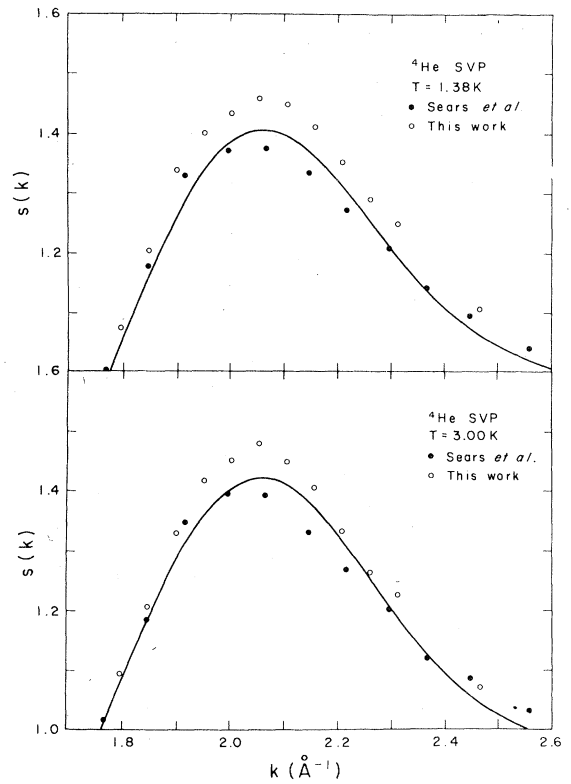

FIG. 19. Comparison between $S_{T2}(k)$(——) and the data for $S(k)$ obtained directly in this work and in Ref. 39.

of the integral at large values of k. In any event it is seen that our results for S_{T2} more closely meet the sum rule test than do the original liquid structure factor values obtained directly from the experiments. The final columns in the table are the consistency integral for a composite structure factor which we discuss in Appendix A and the neutron results of Ref. 39.

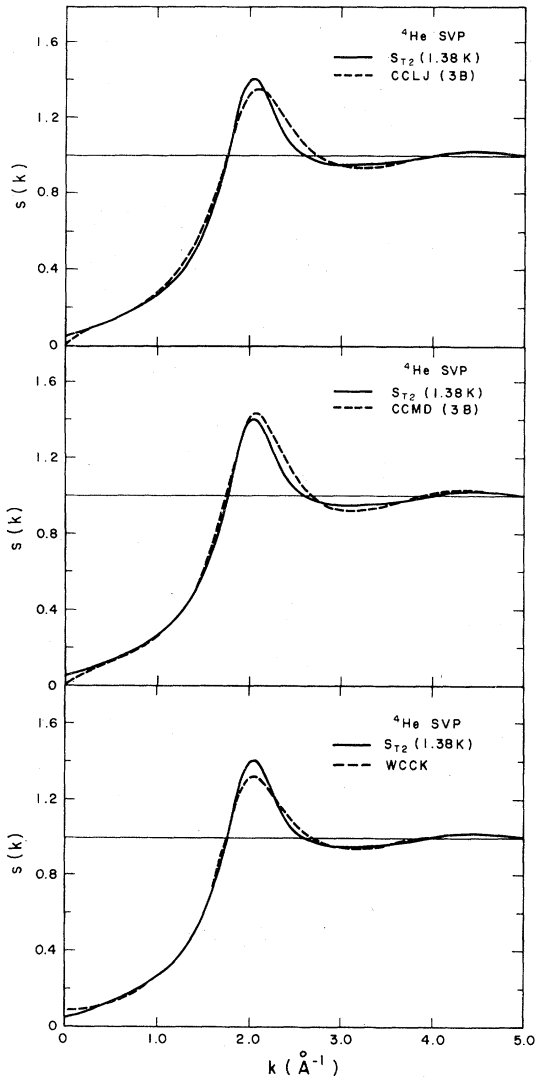

FIG. 20. The liquid structure factor $S_{T2}(k)$ compared to the theoretical calculations of Chang and Campbell (Ref. 50) and Whitlock *et al.* (Ref. 51).

TABLE VI. Values of the integral consistency condition [Eq. (7)] for the various structure factors discussed in the text. The subscripts refer to integrals performed with the various data: S, the smoothed structure factor values [$S_S(k)$] for this work; $T2$, the twice transformed values [$S_{T2}(k)$]; N, the smoothed structure factor values from Ref. 39; C the composite made from $S_{T2}(k)$ and the data of Ref. 39.

T	I_S	I_{T2}	I_N	I_C
1.38	−0.34	−0.74	−0.60	−0.67
1.67	−0.21	−0.66	· · ·	· · ·
2.20	−0.79	−0.68	· · ·	· · ·
2.50	−0.21	−0.73	· · ·	· · ·
3.00	−0.74	−0.60	−0.76	−0.68
3.50	+0.29	−0.54	· · ·	· · ·
4.26	+0.53	−0.73	−0.26	−0.74

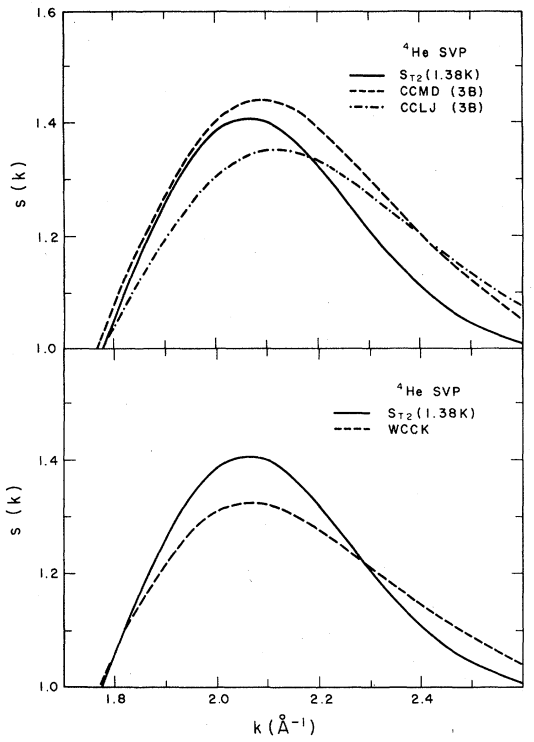

FIG. 21. Similar to Fig. 20 except limited to the region of the structure factor principal maximum.

V. CONCLUSION

We have obtained the structure factor of ^{4}He for several temperatures between 1.38 and 4.24 K. Comparison with available theories suggests the importance of three-body correlations in a complete microscopic theory of liquid ^{4}He. As well, the Lennard-Jones potential does not appear to be as satisfactory as more recent potentials for describing the interatomic interaction in liquid helium. A clear decrease in the structure factor is found to occur on cooling through the λ point.

This work is part of a continuing effort to investigate the structure factor of the quantum fluids. Additional results for elevated pressures will be presented separately. Currently the apparatus is being reconstructed so as to operate at lower temperatures. This will allow additional studies in ^{4}He as well as in ^{3}He and ^{3}He-^{4}He mixtures.

ACKNOWLEDGMENTS

The essential participation of B. L. Weiss in the construction of the apparatus is greatly acknowledged. We are indebted to D. A. Ewen for extensive assistance with the data manipulation. P. D. LePell assisted with some of the data collection. This work was supported by the National Science Foundation through Grants No. DMR 75-08530, No. 77-07727, and No. 79-09248. A grant of computer time from the University Computing Center is acknowledged.

APPENDIX A

We have computed a composite structure factor S_C from the measured structure factor values as smoothed both for the present work and the neutron

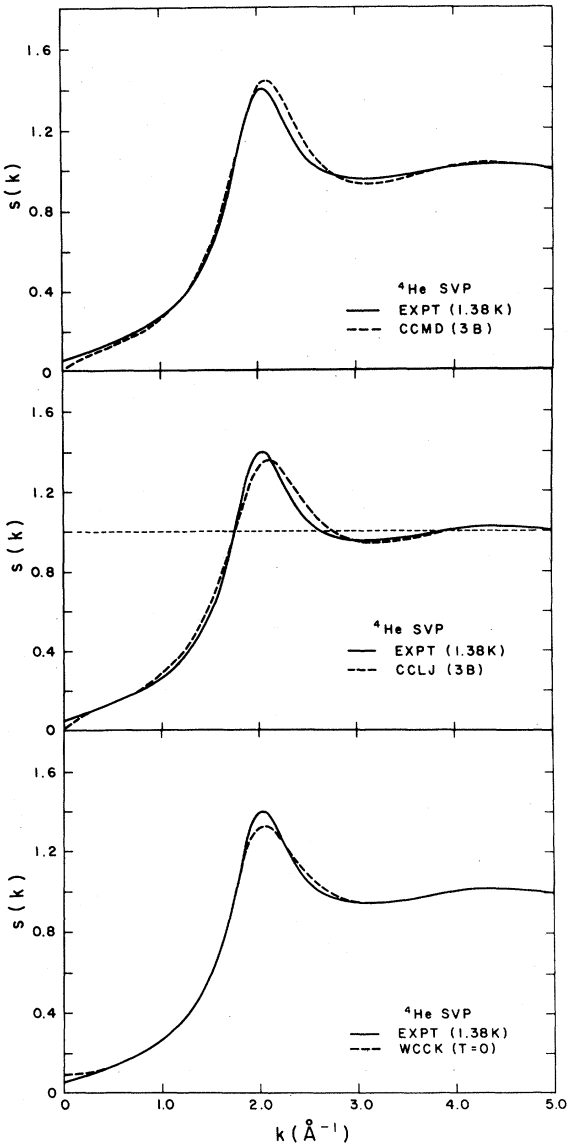

FIG. 22. Comparisons between the composite, S_C, structure function (formed from S_{T2} and the data from Ref. 39 as described in the text) and the theoretical work. In the figures EXPT refers to the composite structure function, S_C.

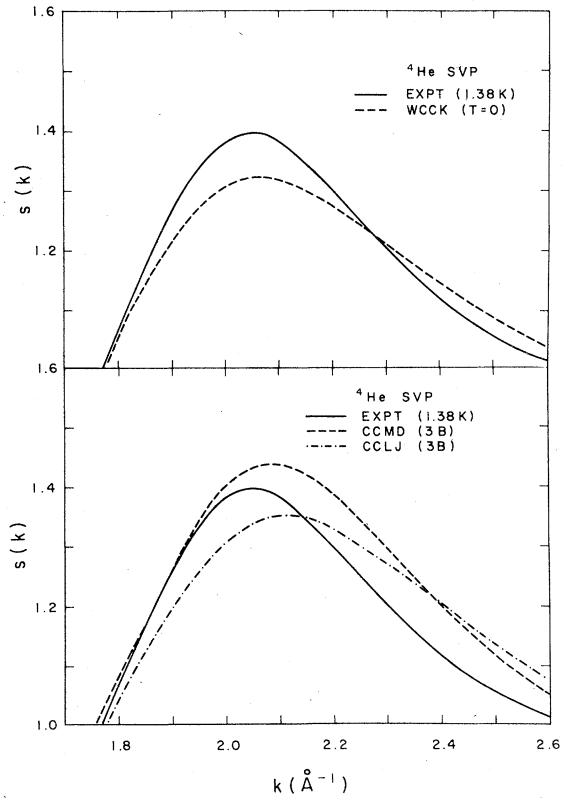

FIG. 23. Similar to Fig. 22 except limited to the region of the structure factor peak.

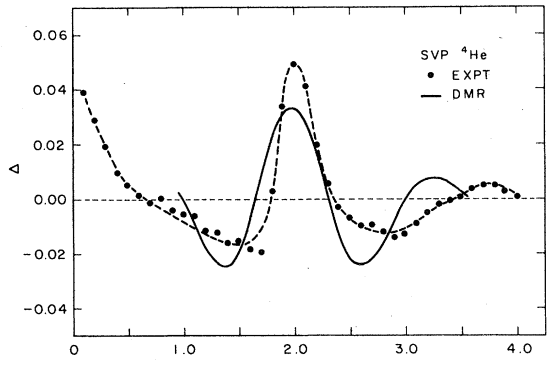

FIG. 24. The difference function $\Delta = S_C(T \simeq 2.23\ \text{K}) - S_C(T = 1.38\ \text{K})$ as a function of momentum transfer. $S_C(k)$ is the composite structure factor formed from $S_{T2}(k)$ and Ref. 39. The solid line is a result of the work of de Michelis *et al.* (Ref. 52). The dashed curve is a guide to the eye.

work of Sears *et al.* To carry this out we have used the structure factor values obtained in this work for $k \lesssim 1$ Å^{-1} and used the average of our $S_{T2}(k)$ values and the neutron smoothed structure factor values for $1 < k \lesssim 5$ Å^{-1}. These results are shown for the case of $T = 1.38$ K in Fig. 22 in comparison to the theoret-

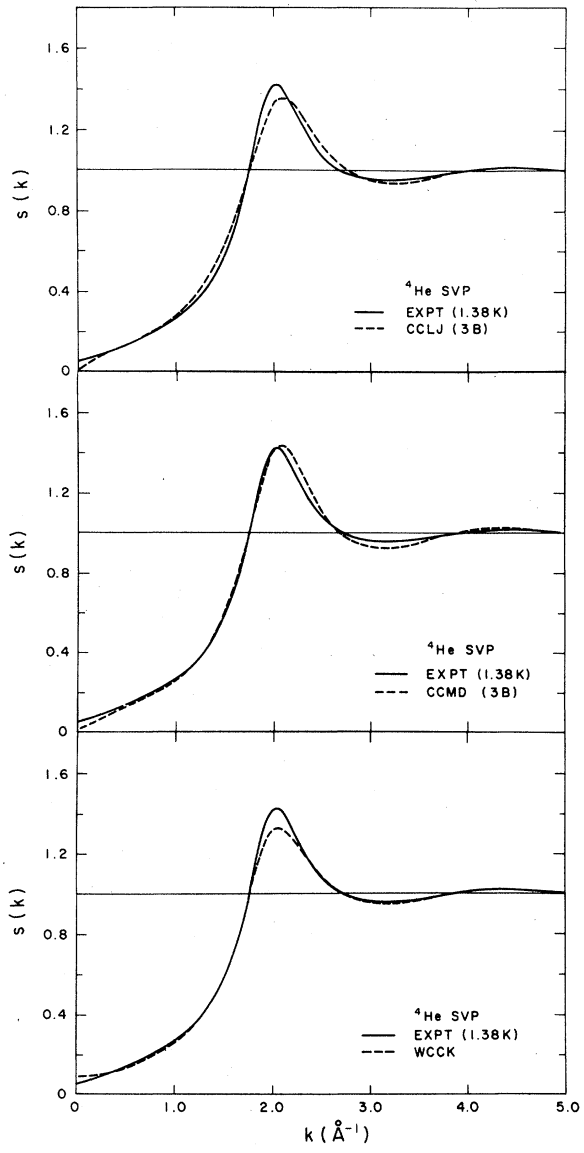

FIG. 25. Comparisons between the theoretical predictions (dashed curves) and the composite structure labeled (EXPT) factor formed from an average of $S_S(k)$ and the data of Ref. 39. Below $k = 1$ Å^{-1} no average is done and the data are due to $S_S(k)$ alone.

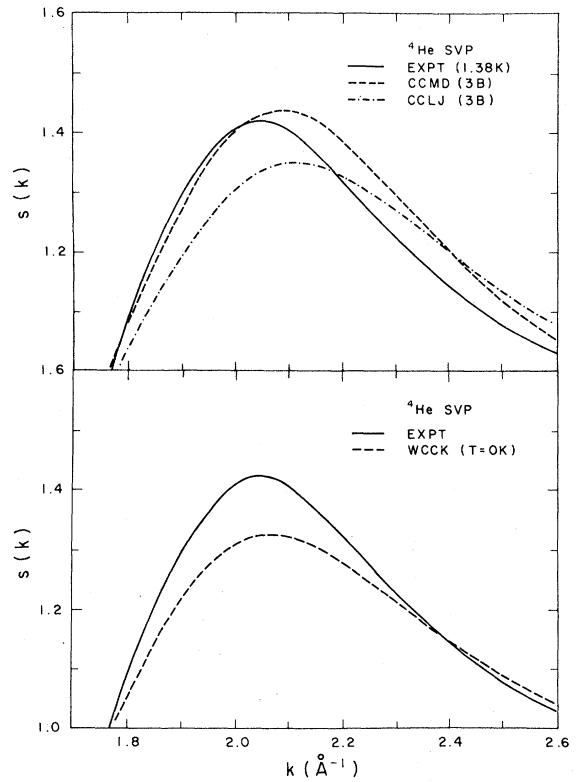

FIG. 26. Similar to Fig. 25 except limited to the structure-factor peak.

ical work of Whitlock *et al.*[51] and Chang and Campbell.[50] The peak region is shown in more detail in Fig. 23 where comparison is made to the theories of Whitlock *et al.*[51] and Chang and Campbell.[50] A general conclusion to be reached is that the Leonnard-Jones potential is inadequate to describe the composite structure factor—it produces a structure factor which is both lower and broader than the experimental values. The MDD2 potential produces again a structure factor which is too broad but in this case higher than the composite experimental values.

The composite structure factor can be compared with the predictions of Reatto and co-workers concerning the change in the structure factor brought about by a change in temperature across T. In Fig. 24 is shown (solid curve) $\Delta = S(T_\lambda) - S(T=0)$ as predicted by the theory and $\Delta = S_C(T \simeq 2.23\ \text{K}) - S_C(T = 1.38\ \text{K})$ as determined from the composite smoothed neutron and x-ray structure factors. The $T = 2.27$ K neutron data and the $T = 2.20$ K x-ray data were used to obtain $S_C(T \simeq 2.23\ \text{K})$.

A second type of composite structure factor can be formed from the data obtained in this work and in Sears *et al.* Rather than use the transformed structure factor S_{T2} one can simply average the neutron results with S_S over the interval $1 \leq k \leq 5$ Å^{-1}. Figures based on this alternate method of forming the composite structure factor are shown in Figs. 25 and 26.

---

*Present address: Mount Holyoke College, South Hadley, Massachusetts.

[1]See, for example, A. H. Compton and S. K. Allison, *X-Rays in Theory and Experiment* (Van Nostrand, New York, 1935).

[2]See, for example, M. S. Green, *The Molecular Theory of Fluids* (North-Holland, Amsterdam, 1952); P. A. Egelstaff, *An Introduction to the Liquid State* (Academic, London, 1967); C. Croxton, *Liquid State Physics* (Cambridge University Press, London, 1974).

[3]N. S. Gingrich, Rev. Mod. Phys. 15, 90 (1943).

[4]H. N. Robkoff, B. L. Weiss, and R. B. Hallock, Rev. Sci. Instrum. (in press).

[5]Rigaku RU-200 PL (copper anode).

[6]Princeton Gamma Tech, intrinsic germanium detector.

[7]Reuter Stokes Xe-CO_2 proportional counter.

[8]Brush Wellman Corp., Los Angeles, California.

[9]The modifications include copper buss bars from the cryogenic reservoirs through the Dewar tail flanges. They also include a copper collar which keeps the upper neck of the ^{4}He reservoir at $\simeq 80$ K independent of the liquid-nitrogen level.

[10]Cryocal Inc. model.

[11]A. G. Tweet, Phys. Rev. 93, 15 (1954).

[12]R. B. Hallock, Phys. Rev. Lett. 23, 830 (1969).

[13]E. K. Achter and L. Meyer, Phys. Rev. 188, 291 (1969).

[14]I. A. Blech and B. L. Averbach, Phys. Rev. 137, A113 (1965).

[15]B. N. Brockhouse, L. M. Corliss, and J. M. Hastings, Phys. Rev. 98, 1721 (1955).

[16]Y. K. Kim and M. Inokuti, Phys. Rev. 165, 39 (1967).

[17]M. L. Rustgi, M. M. Shukla, and A. N. Tripathi, Acta Crystallogr. 16, 926 (1963).

[18]C. Tovard, D. Nicolas, and M. Rouault, J. Chem. Phys. 64, 540 (1967).

[19]J. H. Hubbell, W. J. Veigele, E. A. Briggs, R. T. Brown, D. T. Cromer, and R. J. Howerton, J. Phys. Chem. Ref. Data 4, 471 (1975).

[20]E. O. Wollan, Phys. Rev. 37, 862 (1931).

[21]S. C. Smelser, Ph.D. dissertation (California Institute of Technology, 1969) (unpublished).

[22]J. Maynard, Phys. Rev. B 14, 3868 (1976).

[23]R. D. McCarty, J. Phys. Chem. Ref. Data 2, 293 (1973).

[24]D. L. Elwell and H. Mery, Phys. Rev. 164, 245 (1967).

[25]J. H. Dymond and E. B. Smith, *The Virial Coefficients of Gases* (Oxford University Press, London, 1969).

[26]B. L. Weiss, Ph.D. dissertation (University of Massachusetts, 1977) (unpublished).

[27]H. H. Paalman and C. J. Pings, J. Appl. Phys. 33, 2635 (1962).

[28]P. G. Mikolaj, Ph.D. dissertation (California Institute of Technology, 1965) (unpublished).

[29]*International Tables for X-Ray Crystallography,* edited by K. Lonsdale (Kynoch, Birmingham, 1962).
[30]W. H. McMaster, N. Del Grande, J. H. Mallett, and J. H. Hubbell, Univeristy of California, Lawrence Livermore Laboratory Report No. UCRL-50174 (unpublished).
[31]J. H. Hubbell, At. Data 3, 241 (1971).
[32]B. Mozer, L. A. De Graaf, and B. Le Neindre, Phys. Rev. A 9, 448 (1974).
[33]See, for example, L. Goldstein, Phys. Rev. 84, 446 (1951).
[34]R. P. Feynman and M. Cohen, Phys. Rev. 102, 1189 (1956).
[35]W. L. Gordan, C. H. Shaw, and J. G. Daunt, J. Phys. Chem. Solids 5, 117 (1958).
[36]C. F. A. Beaumont and J. Reekie, Proc. R. Soc. London Ser. A 228, 363 (1955).
[37]D. G. Henshaw, Phys. Rev. 119, 9 (1960).
[38]D. G. Hurst and D. G. Henshaw, Phys. Rev. 100, 994 (1955).
[39]V. F. Sears, E. C. Svensson, A. D. B. Woods, and P. Martel, Atomic Energy of Canada Ltd. Report No. AECL-6779 (unpublished).
[40]E. C. Svensson, V. F. Sears, A. D. B. Woods, and P. Martel, Phys. Rev. B 21, 3638 (1980).
[41]H. N. Robkoff and R. B. Hallock (unpublished). This work contains an extensive set of measurements at elevated pressures.
[42]R. B. Hallock, Phys. Rev. A 5, 320 (1972).
[43]W. L. McMillan, Phys. Rev. 138, A442 (1965).
[44]C. E. Campbell and E. Freenberg, Phys. Rev. 188, 396 (1969).
[45]H. W. Jackson and E. Feenberg, Ann. Phys. (N.Y.) 15, 266 (1961).
[46]E. Muron, Phys. Fluids 1, 139 (1958); T. Morita, Prog. Theor. Phys. (Kyoto) 20, 920 (1958).
[47]J. K. Percus and G. J. Yevick, Phys. Rev. 110, 1 (1958).
[48]W. P. Francis, G. V. Chester, and L. Reatto, Phys. Rev. A 1, 86 (1970).
[49]C. de Michelis and L. Reatto, Phys. Lett. 50A, 275 (1974).
[50]C. C. Chang and C. E. Campbell, Phys. Rev. B 15, 4238 (1977).
[51]P. A. Whitlock, D. M. Ceperley, G. V. Chester, and M. H. Kalos, Phys. Rev. B 19, 5598 (1979).
[52]C. de Michelis, G. L. Masserini, and L. Reatto, Phys. Lett. 66A, 484 (1978).
[53]C. de Michelis, G. L. Masserini, and L. Reatto, Phys. Rev. A 18, 296 (1978).
[54]G. Galione, G. L. Masserini, and L. Reatto (unpublished).
[55]R. D. Murphy, Phys. Rev. A 5, 331 (1972).
[56]D. E. Beck, Mol. Phys. 14, 311 (1968).
[57]L. W. Bruch and I. J. McGee, J. Chem. Phys. 46, 2959 (1967); 52, 5884 (1970).
[58]M. H. Kolos, D. Levesque, and L. Verlet, Phys. Rev. A 9, 2178 (1974).
[59]F. W. Cummings, G. J. Hyland, and G. Rowlands, Phys. Kondens. Mater. 12, 90 (1970).
[60]G. J. Hyland, G. Rowlands, and F. W. Cummings, Phys. Lett. A 31, 465 (1970).
[61]H. N. Robkoff, D. A. Ewen, and R. B. Hallock, Phys. Rev. Lett. 43, 2006 (1979).
[62]V. F. Sears and E. C. Svensson, Phys. Rev. Lett. 43, 2009 (1979).
[63]A. L. Fetter (unpublished) and (private communications).
[64]A. Griffin (unpublished).